

---

**This manuscript is a EarthArXiv preprint** and has been submitted for publication in the **Journal of the Geological Society**. Please note that the manuscript has been peer-reviewed but not yet formally accepted for publication. Subsequent versions of this manuscript may, thus, have slightly different content. If accepted, the final version of this manuscript will be available via the 'Peer-reviewed Publication DOI' link on the right-hand side of this webpage. Please feel free to contact any of the authors; we welcome feedback.

---

# The enigma of the Albian Gap: spatial variability and the competition between salt expulsion and extension

Leonardo M. Pichel\* and Christopher A-L. Jackson

Basins Research Group (BRG), Department of Earth Science and Engineering, Imperial College  
London, South Kensington Campus, SW7 2BP, United Kingdom

\* [l.muniz-pereira@imperial.ac.uk](mailto:l.muniz-pereira@imperial.ac.uk)

The Albian Gap is a uniquely large (up to 65 km wide and >450 km long), enigmatic salt-related structure in the Santos Basin, offshore Brazil. It is located near the basin margin and trends NE (i.e. sub-parallel to the Brazilian coastline). The gap is characterized by a near-complete absence of Albian strata above depleted Aptian salt. Its most remarkable feature is an equivalently large, equally as enigmatic, basinward-dipping, supra-salt rollover that contains a post-Albian sedimentary succession that is up to 9 km thick. Due to its unique geometry, size, and counter-regional aspect, the origin and evolution of the Albian Gap has been the centre of debate for >25 years. This debate revolves around two competing models; i.e. did it form due to thin-skinned (i.e. supra-salt) extension, or progradational loading and salt expulsion? The extension-driven model states that the Albian Gap (and overlying rollover) formed due to post-Albian gravity-driven extension accommodated by slip on a large, counter-regional, listric normal fault (the Cabo Frio Fault). Conversely, the expulsion-driven hypothesis states that the Albian Gap was established earlier, during the Albian, and that post-Albian deformation was controlled by differential loading, vertical subsidence, and basinward salt expulsion in the absence of significant lateral extension. This study utilizes a large (c. 76,000 km<sup>2</sup>), dense (4-8 km line spacing), depth-migrated, 2D seismic dataset that fully covers and thus permits, for the first time, a detailed, quasi-3D structural analysis of the entire Albian Gap. In this study we focus on: i) the evolution of base-salt relief and the original salt thickness variations; and ii) the geometry of the post-Albian rollover, and its related faults and salt structures. To constrain the kinematics of the Albian Gap, and how this relates to the evolution of the base-salt relief, we also apply novel structural restoration workflows that incorporate flexural isostasy, in addition to a detailed, sequential reconstruction of the intra-gap rollover sequences. Our results show that the geometry and kinematics of the Albian Gap vary along-strike, and that both post-Albian extension *and* expulsion play a

significant role in its evolution. Basinward-dipping growth wedges, salt rollers, and listric normal faults record extension, whereas sigmoidal wedges, halokinetic sequences, and upturned near-diapir flaps, the latter two associated with large diapirs bounding the downdip edge of the gap, record basinward salt expulsion and inflation. Where the Albian gap is relatively wide (>50 km), these processes alternate and operate at approximately equal proportions. Our results are consistent with the amount of basinward translation inferred from the analysis of ramp-syncline basins located downdip on the São Paulo Plateau. Our results seemingly reconcile one of the longest-running debates in salt tectonics, as well as having more general implications for understanding the regional kinematics and dynamics of salt-related structures in other salt basins, in particular the controls on the development of large, counter-regional faults.

## 1 **1. Introduction**

2 Salt-bearing passive margins are typified by kinematically-linked domains of updip  
3 extension, midslope translation, and downdip contraction and/or salt advance (e.g.  
4 Rowan et al., 2004; Peel 2014; Jackson et al., 2015; Jackson and Hudec, 2017). Each  
5 of these domains are associated with a complex and variable suite of salt structures.  
6 Updip areas of extension are characterized by reactive diapirs, salt rollers, and salt-  
7 detached, listric normal faults, whereas downdip areas of contraction are dominated  
8 by salt-cored (buckle) folds, thrusts, and actively rising, squeezed diapirs. Intermediate  
9 translational domains can have both styles of deformation when developed above  
10 variable base-salt relief (Brun and Fort, 2011; Jackson et al., 2015; Dooley et al., 2016;  
11 2018; Pichel et al., 2019b,c). One of the largest and perhaps the most controversial  
12 salt structures worldwide is the Albian Gap in the Santos Basin, Brazil. It trends NE, is  
13 up to 65 km wide in its south-central part, and extends sub-parallel to the Brazilian  
14 margin for nearly the entire length of the Santos Basin (c. 450 km long). The gap is  
15 located at the boundary between the extensional and translational domains, and is  
16 characterized by the near-complete absence of Albian strata and an equally large, up  
17 to 55 km wide, Late Cretaceous-Paleogene counter-regional (i.e. basinward-dipping)  
18 rollover that overlies depleted Aptian salt (Fig. 1) (Demercian et al., 1993; Mohriak et  
19 al., 1995; Davison et al., 2012; Guerra and Underhill., 2012; Fiduk and Rowan, 2012;  
20 Quirk et al., 2012; Jackson et al., 2015).

21 Due to its unique size, geometry and counter-regional aspect, the Albian Gap has  
22 been the centre of debate for >25 years (Fig. 2). This debate revolves primarily around  
23 its origin and evolution, which have been variably described by either an *extension-*  
24 *(Fig. 2a)* and *expulsion-driven model* (Fig. 2b). Many authors propose an extension-

25 driven origin in which the rollover and the gap itself formed due to post-Albian gravity-  
26 driven extension associated with slip on a large, counter-regional, salt-detached  
27 normal fault, the Cabo Frio Fault (CFF, fig. 1), which accommodates 30-55 km of  
28 lateral displacement (i.e. heave; Fig. 2a) (Cobbold and Szatmari, 1991; Demercian et  
29 al., 1993; Mohriak et al., 1995; Davison et al., 2012; Guerra and Underhill., 2012;  
30 Rowan and Ratcliff, 2012; Quirk et al., 2012). Others suggest an expulsion-driven  
31 origin in which the gap was established earlier, during the Albian, and in which post-  
32 Albian deformation was driven by margin progradation and associated differential  
33 loading, vertical subsidence, and basinward salt expulsion. These processes together  
34 generated the post-Albian expulsion rollover characterising the Albian Gap (Fig. 2b).  
35 This model does not require or invoke significant lateral extension or overburden  
36 translation (Szatmari et al., 1996; Ge et al., 1997; Gemmer et al., 2005; Krézsek et al  
37 2007; Adam and Krézsek, 2010; Jackson et al., 2015). Cross-section based  
38 restorations of the Albian Gap have not yet resolved this debate, as the gap can be  
39 reasonably restored either by post-Albian extension (Fig. 2a), or basinward salt  
40 expulsion following Albian diapirism (Fig. 2b) (Rowan and Ratliff, 2012; Jackson et al.,  
41 2015). In the former model (Fig. 2a), the post-Albian rollover is equivalent to the  
42 hangingwall of a counter-regional, salt-detached normal fault, with diapirs and  
43 minibasins in its footwall translating basinward for a distance equal to the fault heave.  
44 In the latter model (Fig. 2b), the rollover is restored by basinward salt expulsion from  
45 a diapir that decreases in width through time, and in which there is no lateral movement  
46 of basinward minibasins and associated salt structures.

47 These two competing hypotheses are intrinsically related to another long-lived  
48 controversy, the general salt tectonics and structural evolution of the São Paulo  
49 Plateau, a large, basement-cored structural high located immediately downdip of the

50 Albian Gap (Fig. 1b). In the extension-driven model, post-Albian extension within the  
51 Albian Gap is kinematically balanced by the lateral movement of salt and its  
52 overburden on the São Paulo Plateau and downdip contraction of the overburden  
53 and/or salt advance via nappe emplacement (Guerra and Underhill, 2012; Fiduk and  
54 Rowan, 2012; Quirk et al., 2012; Rowan and Ratliff, 2012). Conversely, in the  
55 expulsion-driven model, post-Albian deformation is characterized by salt inflation and  
56 intense, intra-salt deformation, but *not* significant overburden translation and  
57 contraction (Ge et al., 1997; Gemmer et al., 2004; Jackson et al., 2015a,b).

58 Solving these debates is crucial to our understanding of the regional kinematics and  
59 geodynamic evolution of not only of the Santos Basin, but also other salt-bearing  
60 passive margins. Selecting their appropriate kinematic model will help us geometrically  
61 balance basin-scale deformation, and constrain the timing, style, and magnitude of  
62 salt movement, deformation, and sub-horizontal translation, the latter typically being  
63 problematic due to cryptic diapir shortening and extension (Hossack et al., 1995;  
64 Rowan and Ratliff., 2012; Jackson et al., 2015a). Understanding when and how salt  
65 and its overburden deforms has important implications for hydrocarbon exploration  
66 along salt-bearing margins, given it can help us constrain the location and timing of  
67 hydrocarbon migration and trap formation, and the timing of deposition of key  
68 petroleum system elements (e.g. source, reservoir, and seal rocks; Jackson et al.,  
69 2015; Allen et al., 2016; Pichel et al., 2018). In addition, similar kilometre-scale  
70 counter-regional rollovers, geometrically similar to the one in the Santos Basin, are  
71 recognized in the northern Gulf of Mexico (Hudec et al., 2019; C. Rodriguez, pers.  
72 comm, 2020) and in the Kwanza Basin, offshore Angola (Legeay et al. 2019); in both  
73 these locations, the origin of the rollovers is still debated.

74 In this study, we present, for the first time, a detailed geometric and kinematic analysis  
75 of nearly the entire Albian Gap (Figs. 1 and 3). Whereas most previous studies focused  
76 on only one or two, dip-orientated (i.e. NW-trending) cross sections through the centre  
77 of the gap where it is widest (Demercian et al., 1993; Mohriak et al., 1995; Ge et al.,  
78 1997; Fiduk and Rowan, 2012; Guerra and Underhill, 2012; Jackson et al., 2015), we  
79 analyse several dip- and strike-oriented sections to understand its true 3D geometrical  
80 and possibly kinematic variability. We use an extensive and modern, 2D depth-  
81 migrated seismic dataset (Fig. 1). Small 2D line spacing (4-8 km) provides a dense,  
82 quasi-3D grid with which to analyse lateral and vertical variations in base-salt relief,  
83 salt and growth strata geometries, and overburden faulting within the Albian Gap. In  
84 addition, we restore three cross-sections from different parts of the Albian Gap,  
85 focusing on the overlying post-Albian rollover, bounding salt structures, and  
86 detachment geometry. By doing this, we are able to constrain the contribution of  
87 different mechanisms (i.e. extension and expulsion) to the formation of the gap and,  
88 we hope, solve one of the longest-lived controversies in salt tectonics.

## 89 **2. Geological Setting**

90 The Santos Basin covers c.  $3.5 \times 10^5$  km<sup>2</sup> and is bound by the Cabo Frio High to the  
91 northeast and by the Florianopolis Platform to the southwest (Mohriak et al., 1995;  
92 Garcia et al., 2012) (Fig. 1a). The basin originated as a rift during the Early Cretaceous  
93 in response to the opening of the South Atlantic (Fig.1a-b) (e.g., Meisling et al., 2001;  
94 Modica and Brush, 2004; Karner and Gambôa, 2007; Mohriak et al., 2008). Grabens  
95 and half-grabens were oriented predominantly NNE-NE due to ESE-SE directed  
96 extension and were filled by largely Barremian, fluvial-lacustrine deposits that are  
97 overlain by an early-to-middle Aptian, carbonate-dominated succession (Meisling et  
98 al., 2001; Davison et al., 2012). The number of active faults and their rate of slip

99 decreased during the Aptian and, by the Late-Aptian, a c. 2.5-4 km thick salt  
100 succession was deposited (Fig. 1c) (De Freitas, 2006; Davison et al., 2012; Garcia et  
101 al., 2012). Salt deposition was controlled by an inherited rift topography, resulting in  
102 marked spatial variations in original salt thickness (Davison et al., 2012; Garcia et al.,  
103 2012; Rodriguez et al. 2018). In sub-salt lows such as the Merluza Graben (Fig. 1c)  
104 (cf. Mohriak et al., 2010), salt was up to c. 4 km thick (Garcia et al., 2012; Lebit et al.,  
105 2019). Conversely, on sub-salt highs such as the Outer High (Fig. 1c), salt was only  
106 c. 1.5-2 km thick (Garcia et al., 2012; Rodriguez et al., 2018).

107 During the early Albian, the Santos Basin experienced fully marine conditions due to  
108 thermally induced, post-rift subsidence and a rise in eustatic sea-level (drift stage, Fig.  
109 1b). This resulted in widespread deposition of a carbonate-dominated succession that  
110 was up to c. 1 km thick updip and which thinned basinward to c. 200 m on the São  
111 Paulo Plateau (Fig. 1c) (Modica & Brush, 2004). During the late Albian, the basin tilted  
112 south-eastward, inducing gravity gliding of the salt and its overburden. Salt-related  
113 deformation produced numerous thin-skinned, predominantly basinward-dipping, salt-  
114 detached normal faults that dismembered the Albian carbonate platform into rafts in  
115 the updip extensional domain (zone of extension, fig. 1) (Demercian et al., 1993;  
116 Cobbold et al., 1995; Guerra and Underhill, 2012; Quirk et al., 2012). The Albian Gap,  
117 the focus of our study, is located at the basinward (i.e. south-eastern) edge of the  
118 extensional domain (Fig. 1).

119 Post-Albian sedimentation was characterized by margin-scale clastic progradation,  
120 with sediments derived from the uplifting of the Serra do Mar mountain range (Fig. 1a-  
121 b) (Modica & Brush, 2004). Most late Albian faults in the updip extension domain  
122 became inactive by the end of the Albian and deformation migrated downdip into the  
123 Albian Gap and onto the São Paulo Plateau (SPP) (Fig. 1) (Quirk et al., 2012; Jackson



124 et al. 2015a). Post-Albian salt tectonics was characterized by basinward salt  
125 evacuation from the Albian Gap, local salt welding (Davison et al., 2012; Jackson et  
126 al., 2014; 2015a), and up to c. 30 km of overburden translation further downdip in the  
127 São Paulo Plateau (Fig. 1c) (Pichel et al., 2018; 2019c). The base-salt relief and salt  
128 thickness variations associated with the inherited rift topography impacted salt  
129 tectonics on the São Paulo Plateau, generating flow partition with localized  
130 contraction, extension and passive diapirism (Garcia et al., 2012; Pichel et al., 2018;  
131 2019c).

### 132 **3.1 Dataset and Methods**

#### 133 **3.1. Seismic Data and Interpretation**

134 We use a vast (c. 76,000 km<sup>2</sup> areal coverage), zero-phased processed, Kirchoff pre-  
135 stack depth-migrated 2D seismic dataset covering nearly the entire length of the  
136 Santos Basin and the Albian Gap (Fig. 1). The 2D survey comprises NW- and NE-  
137 trending profiles that are oriented sub-parallel to the dip- and strike-direction of the  
138 basin (and Albian Gap), respectively (Fig. 1d). Given the size of the Albian Gap, the  
139 seismic dataset has a relatively small line spacing (c. 4 km and 8 km between dip- and  
140 strike-orientated profiles, respectively), giving it a quasi-3D character. Seismic profiles  
141 have a total record length of 16 km and we display images following the Society of  
142 Economic Geologists (SEG) normal polarity convention, whereby a downward  
143 increase in acoustic impedance is represented by a positive reflection event (white on  
144 greyscale seismic sections) and a decrease in acoustic impedance by a negative  
145 event (black on greyscale seismic section) (Brown, 2011). The seismic data almost  
146 fully images the updip extensional domain and partly images the intermediate  
147 translational and minibasin province (cf. Pichel et al., 2018; 2019; Lebit et al 2019),

148 intersecting the updip portion of the 3D seismic dataset used by Jackson et al. (2015b)  
149 and Pichel et al. (2018; 2019) (Fig. 1).

150 We mapped base- and top-salt based on their distinct seismic expression and  
151 overburden geometries (Fig. 3). As we did not have direct access to borehole data,  
152 mapping of key post-salt horizons were based on their tectono- and seismic-  
153 stratigraphic significance, with age-calibration provided by a number of recently  
154 published, borehole-constrained cross-sections (Garcia et al., 2012; Guerra and  
155 Underhill., 2012; Quirk et al., 2012; Hadler-Jacobsen et al., 2014; Jackson et al.,  
156 2015a; Rodriguez et al., 2018). We mapped a Top Albian unconformity (blue) to outline  
157 the geometry and extent of the Albian Gap (Fig. 4), and a prominent Paleogene  
158 regional unconformity (yellow on figure 1b-c and seismic profiles) that marks the end  
159 of bulk salt deformation across most of the basin (cf. Fiduk and Rowan, 2012; Garcia  
160 et al., 2012; Guerra and Underhill, 2012; Jackson et al., 2015b). We also mapped key  
161 post-Albian (Upper Cretaceous-Paleocene) horizons within the Albian Gap rollover to  
162 constrain its present structural style and to infer its evolution via isopach (thickness  
163 map) analysis.

### 164 **3.2. Restorations**

165 To restore geometries imaged on seismic reflection profiles we combine decompaction  
166 and unfolding by simple vertical shear, and move-on-fault algorithms, following  
167 established restoration workflows for salt-related deformation (cf. Rowan and Ratliff  
168 2012). Instead of restoring only a single profile (cf. Ge et al., 1997; Rowan and Ratliff,  
169 2012; Guerra and Underhill, 2012; Jackson et al., 2015), we perform 2D structural  
170 restorations of three of the most representative profiles from the Albian Gap.

171 We restore these profiles to a gently-dipping, clinoform-like seabed that is  
172 characteristic of many prograding clastic slopes (cf. Hadler-Jacobsen et al. 2014); by  
173 doing this, we incorporate geologically more realistic geometries not applied in  
174 previous restorations of the Albian Gap (Fig. 5a). Although commonly gentle (c. 1°),  
175 the foresets of margin-scale prograding clinoforms can reach up to 16° (Patruno et al.,  
176 2015), dipping 0.5-2° and being c. 50-300m tall in the study-area (see present-day  
177 seabed, figs. 6-10). Thus, previous workflows that restored post-Albian rollover  
178 horizons to a flat top (cf. Rowan and Ratliff, 2012; Jackson et al., 2015) have likely  
179 distorted their original geometries, as well as the gap itself, overestimating the amount  
180 of extension. This is seen by differences in geometry, fault heave and throw for the  
181 same wedge restored to a flat datum (8 km heave and 3.75 km throw) or one restored  
182 to a gently-dipping seabed (7.4 km heave and 3.6 km throw) (fig. 5a). We reconstruct  
183 the approximate paleo-seabed through time using the present seabed as template and  
184 local erosional unconformities and toplaps as additional constraints. Although  
185 estimating the bathymetry over time involves some uncertainty, clear stratal  
186 terminations in and around the Albian Gap afford confidence in our workflow and, we  
187 argue, allows a more accurate representation of growth strata geometries than  
188 previous achieved.

189 Decompaction is performed using the Sclater and Christie (1980) function, assuming  
190 a carbonate-dominated (i.e. Albian) and siliciclastic-dominated (i.e. post-Albian)  
191 overburden; this assumption is supported by lithological data provided by boreholes  
192 (Guerra and Underhill, 2012; Hadler-Jacobsen, 2014). This step is important because  
193 it removes the effects of compaction through time, and thereby produces a more  
194 accurate visualization of temporal variations in the original rollover geometries,  
195 thickness and associated fault throw (Fig. 5b).

216 We also incorporate flexural isostatic compensation in each decompaction step to  
217 quantify and remove the effects of differential loading and basin subsidence, which  
218 ultimately provides more accurate estimates of the base-salt geometry, regional dip,  
219 and related salt thickness through time (Fig. 5c). This ultimately permits us to establish  
220 the key boundary conditions governing the evolution of the Albian Gap. We use a  
221 crustal density of  $2.78 \text{ g/cm}^3$  and lithospheric elastic thickness ( $T_e$ ) of 5 km. We also  
222 test  $T_e$  values of 1.5, 10 and 15 km but choose  $T_e = 5 \text{ km}$  as we (and others;  
223 Scotchman et al., 2006; 2010) argue this is a more valid approximation for highly-  
224 stretched continental crust; the same value has been applied by other studies focused  
225 on the geodynamic evolution of the Santos Basin (Garcia et al., 2012; Rodriguez et  
226 al., 2019). We perform a detailed sequential restoration of the central and most  
227 representative section within the Albian Gap involving 12 steps from Aptian (top-salt)  
228 to present. We then restore additional sections back to the Albian and Aptian; this  
229 allows us to constrain spatial variations in the original dimension of the Albian Gap  
230 and the original Aptian salt thickness, and the overall basin geometry and depth.

#### 231 **4. Distinguishing extension from expulsion**

232 Distinguishing between structural geometries formed by extension vs. salt expulsion  
233 is central to determining the processes responsible for the formation of the Albian Gap.  
234 As we will argue below, we find evidence for both extension (Fig. 6a) and salt expulsion  
235 (Fig. 6b) in the Albian Gap (Figs. 7-9), with the distribution, geometry, and stratigraphic  
236 architecture of the related rollover geometries described in the following section  
237 (section 5). However, in order to provide a geometric framework within which to  
238 interpret our data, we first briefly review the types of rollover geometries produced in  
239 physical models of extension- and expulsion-related salt tectonics, as well as those

220 identified in natural examples (Fig. 6) (cf. Jackson and Hudec, 2017 and references  
221 therein).

222 We recognize three rollover-related structural styles diagnostic of salt-detached  
223 extension: i) salt rollers, ii) salt-detached normal faults and, iii) their associated wedge-  
224 shaped growth strata, which thicken towards and are thickest immediately adjacent to  
225 the fault and/or flanking diapir (where present) (Figs. 6a and 7-9) (cf. Mauduit et al.,  
226 1997; Chimney and Kluth, 2002 Brun and Mauduit, 2009; Jackson and Hudec, 2017).  
227 To estimate the amount of extension during deposition of any given sequence, and  
228 thus within each time-step in our restorations, we: i) measure fault heave where  
229 corresponding footwall *and* hangingwall cut-offs are unambiguously observed (Figs. 7  
230 and 9); or ii) use the width of their hangingwall growth section (cf. heave in fig. 5a).

231 In the case of differential loading and basinward salt expulsion, we identify three key  
232 rollover-related structural styles: i) sigmoidal wedges that thicken and then thin in the  
233 direction of salt expulsion, typically towards and onlapping onto a bounding diapir (Fig.  
234 6b), ii) significant downdip salt inflation, and iii) halokinetic sequences and/or upturned  
235 flaps flanking the rollover-bounding diapir (Figs. 7-9). As these expulsion rollovers  
236 evolve and underlying salt deflates, older sequences rotate downwards and may not  
237 presently be upturned, instead displaying a sigmoidal shape defined by basinward  
238 stratal thinning towards a sub-horizontal salt contact (Fig. 6b).

239 Previous quantitative analysis of the post-Albian rollover in the Albian Gap (cf. Ge et  
240 al., 1997; Jackson et al., 2015a) show an asymmetric dip-depth relationship for its  
241 growth strata, arguing against a purely extensional origin for the feature, and thus  
242 suggesting some contribution of loading-driven, expulsion-related processes. Other  
243 studies document c. 28-32 km of post-Albian basinward translation of salt and  
244 overburden within RSBs immediately downdip of the Albian Gap (Pichel et al., 2018),

245 also arguing against a purely expulsion origin and therefore indicating also that  
246 extensional processes also occurred.

247 Although presented as end-member types, the dynamic and kinematic models outlined  
248 above can operate simultaneously. The stratal thickening associated with extension-  
249 driven rollovers tends to generate differential loading of underlying salt, and greater  
250 subsidence and salt expulsion beneath the hangingwalls of their bounding faults.  
251 Conversely, expulsion-driven wedges may also accommodate some sub-horizontal  
252 extension on secondary normal faults, or against the downdip salt wall, especially  
253 when they are deposited above basinward-dipping salt-detachments (sigmoidal  
254 wedges offset by older faults in fig. 7, or wedges terminating against small normal  
255 faults in Fig. 8). For these reasons, we mapped post-Albian rollover wedges based  
256 *purely* on their large-scale geometry (i.e. sigmoidal vs. basinward-thickening),  
257 informed by geometries observed in physical models and other natural examples, but  
258 without a preferred kinematic or dynamic model in mind. We then use these  
259 geometrical constraints in our cross-sectional restorations to quantify the contribution  
260 of extension vs. expulsion to the formation of the Albian Gap. However, given the two  
261 end-member processes are intrinsically-linked, there is some error in our estimates  
262 (i.e. a period dominated by expulsion includes some extension). Constraining this  
263 estimate is hard (i.e. how *much* extension occurs during a period otherwise dominated  
264 by expulsion), although it is clear that the thickness of extension- and expulsion-related  
265 wedges is large compared to, for example, the minor amount of fault slip associated  
266 with the latter process. We therefore estimate a relatively small error of  $\pm 10\%$  to each  
267 restoration step, and to our overall estimate of the contribution of each process.

## 268 **5. Albian Gap Structural Framework**

269 The Albian Gap is c. 450 km long. It varies in width from 10-15 km in the northeast  
270 (North Santos Basin) to 30-50 km in its central portion, widening to 65 km in its central-  
271 south portion, before narrowing again to 15 km to the southwest (Figs. 3-4 and 7-13).  
272 The gap is widest (c. 50-65 km) updip of the Sugar-Loaf and Tupi Sub-Highs (cf.  
273 Rodriguez et al., 2018; Pichel et al. 2019), and where it is intersected by a large NNE-  
274 SSW-striking basement-involved fault (i.e. the Merluza Fault, Mohriak et al., 2011) in  
275 the southwest (Figs. 3-4). The gap is associated with a post-Albian, basinward-dipping  
276 rollover that is of equivalent length, 6-10 km thick (Fig. 14a), and up to 55 km wide  
277 (Fig. 7). This rollover overlies salt that is strongly depleted or apparently welded (Fig.  
278 14b). The salt layer ranges from nearly welded in places (<50 m thick) to an average  
279 of 100 m thick and up to 500 m thick salt rollers (Figs. 7-13 and 14b).

## 280 **5.1. Salt and Fault Geometries**

281 Counter to that previously described, the Albian Gap is not defined on its basinward  
282 edge by a single, through-going (i.e. c. 450 km long), landward-dipping listric fault  
283 (Cabo Frio Fault, cf. Mohriak et al., 1995; Guerra and Underhill, 2012; Fiduk and  
284 Rowan, 2012; Quirk et al., 2012). It is instead bound by a series of smaller (4-12 km  
285 long) fault segments and associated salt rollers (Figs. 7-12). Salt rollers occur within  
286 or defining the outboard margin of the Albian Gap (R in figs. 7-12). The ones within  
287 the gap are relatively small (200-500 m tall on average) (Figs. 7-9), although some are  
288 up to 1.2 km tall (Fig. 13). Rollers bounding the basinward side of the gap are larger  
289 (1-1.5 km tall) than those within the gap *but* occur only in the northern and southern  
290 sectors of the structure (Figs. 11-12). These rollers are broadly asymmetric and  
291 triangular in shape, and are commonly defined on their landward sides by landward-  
292 dipping listric normal faults (Figs. 7-10), although basinward-dipping faults also occur  
293 in the north (Fig. 11) and south of the gap (Fig. 12). In some cases, both sides of the

294 salt rollers are flanked by different-age packages of wedge-shaped strata that towards  
295 them. Such geometries have been described by Quirk and Pilcher (2012), who argue  
296 they document a temporal switch in fault polarity from one diapir flank to the other  
297 (Figs. 11-12) (so-called “flip-flop salt tectonics”; Quirk and Pilcher., 2012).

298 The dominant landward-dipping faults contain 0.4-1 km thick, basinward-thickening  
299 wedges in their hangingwall. Equivalent-age strata are thin or absent on their footwalls  
300 (Figs 7-8). Where strata are missing, we estimate fault heaves of c. 2-6 km using the  
301 width of their hangingwall growth wedges. Salt rollers and faults generally become  
302 younger, larger, and display greater displacement basinward as indicated by their  
303 progressively younger growth strata and their shallower tip heights (Figs. 7-10). This  
304 indicates that extension migrated basinward.

305 The basinward limit of the Albian Gap is, therefore, commonly defined by a partially-  
306 to-fully fault-bounded diapir (Figs. 7-8). Where the gap is relatively narrow (<30 km),  
307 the diapir is asymmetric and triangular in cross-section, a geometry characteristic of  
308 reactive (i.e. extensional) diapirs and/or salt rollers (cf. Vendeville and Jackson, 1992;  
309 Jackson and Hudec, 2017) (Figs. 10-11). However, in the central portion of the gap,  
310 where it is relatively wide (>30 km) (Fig. 7-9 and 12), the geometry and size of the  
311 bounding diapir are markedly different and *cannot* be entirely explained by post-Albian  
312 extension. In this location the diapirs are irregular and semi-circular in plan-view,  
313 rather than linear like those seen to the north and south where extension dominates  
314 (Figs. 3b and 14b). The diapirs are 8-12 km wide, up to 4 km tall, and are *partially*  
315 defined by a landward-dipping listric fault on their landward margins (Figs. 7-8). Locally  
316 upturned and thinned strata are also observed near the tops of the diapirs on their  
317 landward margins. In contrast, their basinward margins are *always* flanked by locally  
318 upturned and thinned strata (Figs. 7-8). In other cases, the diapirs are narrower (2-4



319 km wide), taller (>4.5 km) and have upturned and thinned strata on both of its flanks  
320 with no evidence of extension (Fig. 9). This upturned strata can vary from km-scale,  
321 so-called composite halokinetic sequences (i.e. CHSs) (cf. Giles and Rowan 2012;  
322 Pichel and Jackson 2020) or multi-km upturned flaps (cf. 'megaflaps' of Rowan et al.  
323 2016) (Fig. 15). Larger flaps are more common on the basinward flanks of the gap-  
324 bounding diapirs, whereas CHSs typically occur on their landward sides, within the  
325 Albian Gap.

326 Both cases indicate that the diapirs bounding the central and widest portion of the  
327 Albian Gap were largely influenced (Figs. 7-8) and, in places (Fig. 9), driven by a  
328 combination of passive and active salt rise. Active and especially passive rise are load-  
329 driven processes and can thus occur in the absence of extension (Rowan et al., 2003;  
330 Jackson and Hudec, 2017). However, bounding diapirs experienced an early phase of  
331 reactive, extension-driven rise, as indicated by the presence of rollover strata  
332 thickening towards listric normal faults flanking their lower, landward flanks (Figs. 7-  
333 8).

## 334 **5.2. Rollover Geometries**

335 In addition to the intra- and gap-bounding diapirs, the post-Albian rollover geometries  
336 also vary in terms of their geometry and origin (Figs. 7-9). They can be characterized  
337 by i) basinward-thickening wedges that expand towards landward-dipping, salt-  
338 detached (listric) normal faults (Figs. 7-10); or ii) sigmoidal wedges that are thicker in  
339 their centre, but which thin and downlap basinward towards the salt, onto 'stranded',  
340 intra-gap Albian blocks or the footwalls of salt rollers (Figs. 7-9).

341 Whereas the first geometry is readily linked to regional gravity-driven extension (Fig.  
342 6a) (cf. Brun and Mauduit, 1997; Rowan et al., 1999; Jackson and Hudec, 2017), the

343 second cannot be explained by the same process (Fig. 6b) (see section 4). Besides,  
344 similar sigmoidal, basinward-dipping and -thinning wedges occur landward of the  
345 Albian Gap where they clearly downlap the Albian interval (Fig. 8); this geometry  
346 cannot be readily explained by slip on a normal fault or, therefore, record extension.  
347 We interpret that these sigmoidal geometries are associated with prograding  
348 clinofolds that were later rotated by the deflation and basinward expulsion of salt (Fig.  
349 6b) (cf. Ge et al., 1997; Jackson and Hudec, 2017). They occur predominantly in the  
350 central-south portion of the Albian gap where it is widest (>35 km, figs. 7-9). We make  
351 the key observations that the wider the gap, the more abundant are the sigmoidal  
352 wedges, and the larger is the basinward-bounding diapir (Figs. 7-8).

353 The Albian Gap lies downdip of the Serra do Mar mountain range (Fig. 1), which  
354 formed during the Late Cretaceous-Eocene, coeval with the formation of the Albian  
355 Gap rollover (Mohriak et al., 1995; Guerra and Underhill, 2012). Continental uplift  
356 resulted in erosion and basinward progradation clastic sediments into the Albian Gap  
357 (Modica and Brush, 2004; Guerra and Underhill., 2012). Where the gap is wider and  
358 prograding sigmoidal geometries abound (Figs. 7-9), the post-Albian margin  
359 prograded further basinward (Fig. 16). Where the gap is relatively narrow (<35 km),  
360 basinward-thickening wedges dominate, indicating that, in these areas, the gap  
361 formed primarily in response to extension (Figs. 10-11). In summary, there is a positive  
362 relationship between the amount of post-Albian shelf-margin progradation, the amount  
363 of salt expulsion and thinning, and the overall gap width.

### 364 **5.3. Base-salt Structure and Polarity**

365 Throughout most of the Albian Gap, the base of the salt presently dips gently (<1.5°)  
366 landward and salt-detached extension is controlled by landward-dipping normal faults  
367 that are antithetic to the overall basinward direction of gravity-driven transport (Figs.

368 6-9). At its south and north portions, however, this changes. In its northern portion  
369 where it narrows abruptly to <14 km, the gap is bound by a flip-flop roller and a  
370 basinward-dipping normal fault (Fig. 11). In its southernmost portion, basinward of a  
371 major pre-salt rift structure, the Merluza Graben, the Albian Gap is bound on its  
372 basinward side by basinward-dipping, salt-detached normal faults (Fig. 12). The  
373 Merluza Fault has a throw of 3.5 km at the base-salt and is associated with the largest  
374 diapir (c. 8.5 km tall and 10 km wide) within the study-area (and possibly the entire  
375 basin, Fig. 3b). This suggests that the graben was a major structural low prior to and  
376 during (and possibly after) salt deposition, resulting in initially locally thickened salt (c.  
377 2.5-4 km thick). Other small, landward-dipping, basement-involved sub-salt faults  
378 produced 0.5-1 km of structural relief at the base-salt and, thus, contribute to a  
379 regionally rugose base-salt beneath the Albian Gap (Figs. 3a and 7-10).

380 The thicker succession of Aptian salt within the Merluza Graben resulted in: i) partition  
381 of salt flow with increased diapiric rise updip of the Albian Gap and, ii) a locally steeper,  
382 basinward-dipping base-salt within the Albian Gap due to tilting of the footwall of the  
383 Merluza Fault. The large (c. 10 km wide) diapir near the south-eastern edge of the  
384 Merluza Graben produced an additional c. 10 km of separation of the Albian interval  
385 given the diapir was growing *during* the Albian (i.e. Albian strata were not deposited  
386 above it). Further basinward, the steeper basinward-dipping base-salt influenced the  
387 style of salt-detached faulting here, which is predominantly synthetic (i.e. basinward-  
388 dipping) and in marked contrast to other areas of the Albian Gap.

## 389 **6. Restoration**

### 390 **6.1. Kinematics on a salt-detached slope**

391 Previous structural restorations of the Albian Gap were ambiguous, meaning that the  
392 Albian Gap could be restored by purely salt expulsion and vertical subsidence  
393 (expulsion-model), or regional extension (extension-model) (Rowan and Ratliff, 2012;  
394 Jackson et al. 2015). This ambiguity is at least partly due to the fact these restorations:  
395 i) have not incorporated the variable rollover stratal geometries (i.e. sigmoidal  
396 clinofolds associated with margin progradation vs. basinward-thickening wedges  
397 associated with fault slip), ii) incrementally restored the rollover succession to a flat-  
398 top, distorting the original (i.e. syn-depositional) stratal geometries, iii) have not  
399 included the effects of flexural isostasy, keeping the base-salt static through time, iv)  
400 did not incorporate kinematic constraints provided by structural geometries seen  
401 immediately downdip on the São Paulo Plateau. Here we present for the first time, a  
402 detailed sequential restoration of the Albian Gap incorporating these aspects (Fig. 17).

403 In the main restored section (Fig. 8), centrally located within the Albian Gap, the gap  
404 is presently c. 50 km wide. The cumulative heave on faults flanked by basinward-  
405 thickening, fault slip-related wedges documents c. 26 km of post-Albian extension (Fig.  
406 17a-l). This is equivalent to c. 50% of the current width of the gap, demonstrating that  
407 by Albian times the gap was already there in the form of a c. 24 km wide, c. 2.8 km  
408 tall, and 90-100 km long reactive/passive diapir (Fig. 17m). Early post-Albian  
409 sequences (g, h, j and l) were primarily associated with basinward progradation of the  
410 basin margin by clinoform accretion (Figs. 7-9), and vertical subsidence due to salt  
411 thinning and lateral expulsion. Overlying sequences were predominantly affected by  
412 sub-horizontal extension of the overburden (a-f and i; Fig. 17). The restorations also  
413 demonstrate that extension-dominated wedges commonly involve a secondary  
414 component of differential loading and basinward salt expulsion due to hangingwall  
415 stratal thickening (i.e. note progressive salt thinning beneath extensional wedges; fig.

416 17b-f). Conversely, some sigmoidal, expulsion-dominated wedges also demonstrate  
417 a small amount (c. 1-2 km) of extension against the downdip salt wall (Fig. 17g) or,  
418 more commonly, due to ongoing slip on a previously formed fault (Fig. 17h).

419 Additional restored sections in the central portion of the Albian Gap show that post-  
420 Albian extension varied from 26-28 km ( $\pm 2$  km) (Figs. 18 and 19). All restorations  
421 show that where it is presently widest, the gap was already partly formed during the  
422 Albian in the form of a 24-30 km wide passive diapir (Figs. 17 and 18); this diapir was  
423 initially narrower (<2 km) and, likely reactive where the gap is presently narrower (<30  
424 km, fig. 19). Our restorations show that the variable *present width* of the Albian Gap  
425 was primarily controlled by the *original width* of the gap during the Albian (i.e. Albian  
426 diapir). They also show that post-Albian extension in the central portion of the Albian  
427 Gap (figs. 7-10) showed little along-strike variability (26-28 km, according to our  
428 restorations; figs. 17-19). Extension nonetheless varied laterally throughout the full  
429 length of the Albian Gap, being as little as 10-12 km in the northernmost portion where  
430 the gap is presently narrower (Fig. 12). Our measurements of extension agree with  
431 estimates of 28-32 km of post-Albian translation of salt and overburden obtained from  
432 the analysis of ramp-syncline basins downdip on the São Paulo Plateau (Pichel et al.,  
433 2018). We argue that area was kinematically linked to the Albian Gap, being equivalent  
434 to its (mega)footwall.

## 435 **6.2. Loading and Flexural Isostasy**

436 Flexural isostasy is associated with the long-wavelength effects driven by the isostatic  
437 response of the crust to sediment loading (e.g. Roberts et al., 1998; Scotchman et al.,  
438 2008; Garcia et al., 2012). Flexural isostasy assumes that any load on the lithosphere  
439 is supported by flexural bending stresses within the immediate area surrounding the  
440 load. Applying flexural isostasy to structural restorations has been shown to yield the

441 most geologically realistic results in backstripping workflows (Roberts et al., 1998;  
442 Scotchman et al., 2008). In the Santos Basin, the base-salt beneath and near the  
443 Albian Gap presently dips 0.5-1.5° landward for at least 150 km in the dip direction  
444 (Figs. 7-11), with the exception being the more strongly basinward-dipping footwall of  
445 the Merluza Fault in the south (section 5.3, fig. 12). This is anomalous when compared  
446 to the majority of passive margin salt basins such as in Campos and Espirito Santo  
447 basins, offshore Brazil (Mohriak et al., 2012; Davison et al., 2012; Dooley et al. 2016),  
448 West and Northwest Africa (Marton et al., 2000; Tari et al., 2003; 2012; Hudec and  
449 Jackson, 2004; Peel 2014; Pichel et al., 2019), and the Gulf of Mexico (Rowan et al.,  
450 2004; Hudec et al., 2018), where the detachment presently dips regionally basinward.

451 Our restorations show that this somewhat unusual, landward-dipping attitude of the  
452 salt detachment in the Santos Basin relates to the presence of the equally enigmatic  
453 and large (450 km long, up to 55 km wide and 10 km thick), post-Albian rollover  
454 associated with the Albian Gap (Figs. 7-8). The restorations also demonstrate that the  
455 base-salt originally dipped basinward 1.2-1.5° (on average) and that it switched  
456 polarity progressively through time due to proximal loading by the thick, post-Albian  
457 sequence now overlying and filling the Albian Gap (Figs. 17-19). The landward dip of  
458 the base-salt was, nonetheless, established relatively early, during deposition of the  
459 two lowermost post-Albian sequences (Fig. 18). Deposition and thus isostatic loading  
460 were focused within the Albian Gap as salt was being expelled from underneath it. Salt  
461 expulsion and diapir growth basinward of the gap generated a barrier that hindered  
462 the basinward transport of sediment (cf. Modica and Brush, 2004; Hadler-Jacobsen,  
463 2014).

464 Our restorations also show that the original salt thickness was 0.8-1.2 km over pre-  
465 salt highs, 1-2 km in the Albian Gap, and 1.4-2.8 km further downdip and over pre-salt

466 lows (Figs. 17-19). Although involving a degree of uncertainty due to, for example, the  
467 out-of-plane movement of salt (cf. Rowan and Ratliff, 2012), our top-salt restorations  
468 are based on, we argue, valid assumptions that the salt was in depositional connection  
469 across pre-salt highs and that unfolding to a gently ( $<0.5^\circ$ ) basinward-dipping regional  
470 datum is permissible (see Hudec and Norton, 2019; Hudec et al., 2019). Our measured  
471 depositional salt thicknesses are consistent with the estimates of Davison et al. (2012),  
472 Garcia et al. (2012), and Rodriguez et al. (2018).

## 473 **7. Discussion**

### 474 **7.1. Albian Gap kinematics: expulsion vs. extension**

475 We identified three geometries evidence for gravity-driven, salt-detached, post-Albian  
476 extension within the Albian Gap. These are: i) salt rollers, ii) listric normal faults; iii)  
477 basinward-thickening wedges. Moreover, ramp-syncline basins that indicate 28-32 km  
478 of salt-detached basinward translation on the São Paulo Plateau downdip of the Albian  
479 Gap (cf. Pichel et al., 2018) are another diagnostic of equivalent gravity-driven  
480 extension within the Albian Gap as seen from the restorations (Figs. 17-19).

481 Despite the aforementioned evidence for extension, the sum of observed heaves ( $<30$   
482 km) on individual salt-detached normal faults and stratal separations associated with  
483 related salt rollers cannot account for the entire separation of the Albian interval where  
484 the gap is  $>30$  km wide (Figs. 7-9). Moreover, contrasting diapir and related growth  
485 strata geometries suggest an additional control on its evolution. Three other  
486 observations suggest that post-Albian basinward salt expulsion also played a  
487 significant role in the formation of the Albian Gap: i) basinward-thinning sigmoidal  
488 wedges that downlap onto deflated salt and/or remnant (i.e. intra-gap) Albian blocks;  
489 ii) bounding diapirism and salt inflation; and iii) halokinetic sequences or upturned

490 flaps. These features are all driven by vertical subsidence and differential loading,  
491 forming completely independent of extension.

## 492 **7.2. Albian Gap Model**

493 We have argued that the Albian Gap was formed by a combination of thin-skinned  
494 extension and salt expulsion (i.e. differential loading), with these processes operating  
495 in approximately equal proportions during post-Albian times where the gap is widest  
496 (c. 50-60 km). This is equivalent to c. 25-30 km of post-Albian extension in its central  
497 portion, which balances the amount of post-Albian translation recorded in ramp-  
498 syncline basins further basinward on the São Paulo Plateau (28-32 km of translation;  
499 Pichel et al., 2018). We therefore propose a revised, hybrid model for the Albian Gap  
500 in which we combine both processes (Fig. 20).

501 In our model, the gap was formed by: i) post-Albian salt expulsion due to basinward  
502 progradation of a basin margin-attached clastic wedge and differential loading of an  
503 Albian salt wall; the timing and location of sediment input was coeval with and likely  
504 controlled by uplift of the adjacent Serra do Mar (cf. Modica and Brush, 2004), and ii)  
505 broadly coeval extension related to basinward translation and stretching of overburden  
506 above a salt detachment that initially dipped basinward due to post-rift thermal  
507 subsidence (cf. Quirk et al., 2012) (Fig. 20). Post-Albian basinward translation of salt  
508 and overburden occurred downdip (footwall) of the Albian Gap, whereas within the  
509 gap (hangingwall) only the salt translated basinward. The blocks further landward of  
510 the Albian Gap did not move laterally as, by that time, Aptian salt was locally welded  
511 and the base-salt had flipped to dip landward due to isostatic loading by post-Albian  
512 clastic sediments (Fig. 20). This model explains why the gap is wider in its south-  
513 central portion as a result of greater post-Albian salt mobilization basinward, a process  
514 ultimately driven by: 1) greater local salt supply related to the presence of an initially



515 volumetrically larger, Albian salt wall, and 2) greater basinward progradation of post-  
516 Albian clastic sediments.

517 Our model is analogous to the 'heel-keel model' (cf. Krézsek et al., 2007; Jackson and  
518 Hudec, 2017) where there is a switch from early basinward-dipping faulting to later  
519 landward-dipping fault. In our case, during the Albian, extension was accommodated  
520 primarily by basinward-dipping listric faults (Fig. 20b). Continuous sedimentary loading  
521 in their hangingwalls drove salt withdrawal, increasing basal drag and ultimately  
522 stopping the associated thin-skinned deformation (cf. Krézsek et al., 2007). Salt  
523 expulsion from their hangingwalls resulted in salt inflation and a large diapir then  
524 formed further downdip; this diapir acted as topographic high above which no Albian  
525 sediments were deposited (Fig. 20b). This area was then able to move faster than the  
526 updip depleted salt segment. This resulted in additional 26-28 km (Figs. 17-19) of  
527 separation of the Albian interval due to post-Albian progradation above the thicker,  
528 more mobile salt, and the development of counter-regional faults (Fig. 20c-d). Our  
529 estimates of salt-detached extension are fairly consistent in the central part of the  
530 Albian Gap (26-28 km; Fig. 17-19), but decrease north-eastwards (c. 10-14 km; Fig.  
531 11) and south-westward (c. 5-6 km) (Fig. 3). The evidence for expulsion (i.e. sigmoidal  
532 wedges, near-diapir upturned strata, and major salt inflation) also decreases away  
533 from the gap centre (Figs. 10-12), suggesting that this process becomes secondary,  
534 likely as a consequence of less margin progradation and related salt loading (Fig. 16)  
535 and an initially narrower or absent precursor (i.e. Albian) diapir.

536 These counter-regional faults have thin, tabular successions in their footwalls; in some  
537 cases, strata age-equivalent to that observed in their hangingwalls are locally absent,  
538 meaning that their footwall is mostly formed by younger hangingwall growth strata of  
539 a basinward fault (Figs. 7-9). This suggests that these faults formed over inflated salt

540 lacking pre-extension Albian sediments and that their footwall was primarily composed  
541 of salt expelled from beneath their adjacent hangingwalls (Fig. 20b-c). In other words,  
542 the Albian was not deposited uniformly within the study-area and that, by the beginning  
543 of the Late Cretaceous, the Albian Gap was already partially present in the form of a  
544 20-30 km wide passive diapir (Fig. 20; see also restorations in Fig. 17-18). This initial  
545 diapiric gap could be explained by a combination of reactive and passive salt rise  
546 during the Albian (see Jackson et al., 2015). The additional 25-30 km of separation of  
547 the Albian interval was subsequently accommodated by post-Albian extension. This  
548 resulted in the basinward expulsion of salt from within this Albian diapir onto the São  
549 Paulo Plateau, where salt inflation and 28-32 km of translation are observed (Figs. 17-  
550 20) (c.f. Jackson et al., 2015; Pichel et al., 2019c).

### 551 **7.3. Why the predominance of counter-regional faults?**

552 In gravity-driven systems, downdip salt flow over a basinward-dipping detachment  
553 typically results in the extension being preferentially accommodated by synthetic (i.e.  
554 basinward-dipping) normal faults (Brun and Fort, 2011; Quirk et al., 2012; Jackson  
555 and Hudec, 2017). Why was post-Albian extension along most of the extensional  
556 domain in the Santos Basin largely accommodated on counter-regional, landward-  
557 dipping normal faults? Three possible hypotheses may explain this:

- 558 1) Progressive dip reversal of the salt detachment driven by flexural isostasy
- 559 2) Inherited base-salt relief associated with pre-salt rift faults
- 560 3) Rapid margin-scale progradation above thick salt and salt expulsion basinward

561 The anomalous counter-regional dip of the salt detachment within the Albian Gap likely  
562 influenced the style and polarity of overburden faulting, locally favouring antithetic  
563 basal-shear and counter-regional faulting (cf. Brun and Mauduit 2009). However, as

564 seen from our restorations, which explicitly account for flexural isostasy, the  
565 detachment originally dipped basinward so that the early development of counter-  
566 regional faults and basinward-dipping rollover was not controlled by the detachment  
567 dip. The flip in base-salt polarity may, nonetheless, have favoured the development of  
568 larger counter-regional faults later in the history of the Albian Gap, after a significantly  
569 thick overburden succession was deposited within it (Figs. 7-10).

570 The several, predominantly landward-dipping base-salt steps associated with earlier-  
571 formed rift normal faults produced a rugose base-salt that likely influenced the location  
572 and style of supra-salt faulting, as well as local salt rise in the Albian Gap. The  
573 nucleation of salt and supra-salt structures by rift-related base-salt topography is  
574 demonstrated in several studies (Ge et al., 1997; Adam and Krézsek, 2010; Dooley et  
575 al., 2016; 2018; Pichel et a., 2019a,b,c). The base-salt steps within the Albian Gap  
576 may have disturbed net-basinward salt flow, favouring the development of listric  
577 normal faults and salt rollers with the same polarity to the underlying, base-salt relief  
578 that is dominated by landward-dipping steps (Figs. 7-9). However, given that counter-  
579 regional faults also appear above areas with a locally flat base-salt (Figs. 8 and 10),  
580 this effect appears to be secondary.

581 Physical models of salt-detached rollovers have shown that high-sedimentation rates  
582 favour the development of counter-regional (i.e. landward-dipping) faults (Krézsek et  
583 al., 2007). Prograding margins, such as the Santos Basin, have typically high rates of  
584 accommodation generation and sediment input (Modica and Brush, 2004; Hadler-  
585 Jacobsen et al., 2014). In the Albian Gap, an anomalously thick (> 9 km) overburden  
586 was deposited directly above thick (1.5-2 km) salt during the Late Cretaceous-  
587 Paleogene; this was associated with rapid progradation and hinterland uplift in the  
588 Serra do Mar (Fig. 1).

589 We propose that the three mechanisms outlined above jointly influenced the geometry  
590 and kinematics of the Albian Gap. However, we suspect that the main control on the  
591 development of basinward-dipping rollovers and counter-regional faults and,  
592 therefore, the key driver for extension within the Albian Gap was differential loading  
593 associated with progradation above thick, inflated salt (Fig. 20). This resulted in salt  
594 being expelled basinward from beneath prograding clinoforms and from the earlier-  
595 formed diapir, up onto the footwall of counter-regional faults (Figs. 17 and 20).

## 596 **Conclusions**

597 Our study provides the first ever quantification of the contribution between the two  
598 competing processes generating the Albian Gap, expulsion vs extension. This is  
599 based on systematic analysis of the post-Albian rollover spatial variability and  
600 contrasting growth strata geometries, i.e. basinward-thickening strata vs. sigmoidal  
601 clinoform wedges, distribution of normal faults, and different styles of diapirism. We  
602 identify evidence for post-Albian salt-detached extension as well as evidence for salt  
603 expulsion driven by differential loading within the Albian Gap. This shows that neither  
604 pure post-Albian salt expulsion or extension can fully account for the entire separation  
605 of the Albian interval, nor the observed rollover and diapir geometries within the Albian  
606 Gap.

607 We also applied a novel structural restoration methodology that, for the first time,  
608 combines decompaction, flexural isostasy, and unfolding of margin-scale rollover  
609 geometries to a gently-dipping seafloor. This allowed us to provide detailed structural  
610 restorations of key sections and to present more accurate estimates of how  
611 overburden extension, vertical subsidence, base-salt geometry, and salt and  
612 overburden thickness, varied through time. Moreover, we incorporate the contrasting  
613 Albian Gap rollover geometries and measurements of overburden translation from the

614 adjacent São Paulo Plateau as kinematic constraints. We then propose a new model  
615 based on the seismic observations and structural restorations that demonstrates that  
616 the Albian Gap was formed by a combination of post-Albian extension and salt  
617 expulsion at approximately equal proportions where the gap is wider (>50 km). In this  
618 model, the gap was already partially established during the Albian as a 20-30 wide salt  
619 wall. Additional 25-30 km of extension occurred during the post-Albian driven by  
620 margin-scale progradation of sediments over an inflated salt wall, promoting  
621 differential loading and salt expulsion basinward onto the São Paulo Plateau. The  
622 extension was therefore controlled by differential loading and expulsion of salt  
623 basinward, which, coupled with the gradual base-salt dip reversal and presence of  
624 base-salt steps favoured the development of counter-regional faults. This work not  
625 only specifically contributes to the long-lived debate of the origin of the Albian Gap,  
626 but also to our more general understanding of the controls on the development of  
627 large, thin-skinned, counter-regional faults that are common on many salt-bearing  
628 passive margins. In addition, we also develop a novel restoration workflow for gravity-  
629 driven salt deformation that can be applied to many worldwide salt basins.

## 630 **Acknowledgements**

631 First, we thank TGS and WesternGeco as well as individuals in these companies, in special  
632 Kerly Sanchez and Emmi Vargas for granting permission to use seismic data. We also thank  
633 Schlumberger for academic licenses of Petrel and Petex for Move. We thank also Mar  
634 Moragas and Mike Hudec for the very detailed and constructive reviews that greatly  
635 contributed to improve this paper, as well Giovanni Camanni for the editorial handling. We  
636 thank Craig Magee for providing a bathymetric map for figure one. We are also very grateful  
637 for discussions with Frank Peel, Olly Duffy, Gillian Apps and Mark Rowan which significantly  
638 helped developing the concepts behind this paper.

639 **References**

- 640 Allen, H., Jackson, C. A-L., Fraser, A. J. (2016). Gravity-driven deformation of a  
641 youthful saline giant: the interplay between gliding and spreading in the Messinian  
642 basins of the Eastern Mediterranean. *Petroleum Geoscience*, 22(4), 340-356.
- 643 Brown, A. R. (2011). Interpretation of three-dimensional seismic data. Society of  
644 Exploration Geophysicists and American Association of Petroleum Geologists.
- 645 Brun, J. P., Fort, X. (2011). Salt tectonics at passive margins: Geology versus models.  
646 *Marine and Petroleum Geology*, 28(6), 1123-1145
- 647 Cobbold, P. R., Szatmari, P., Demercian, L. S., Coelho, D., Rossello, E. A. (1995).  
648 Seismic and experimental evidence for thin-skinned horizontal shortening by  
649 convergent radial gliding on evaporites, deep-water Santos Basin, Brazil, *in*: Jackson,  
650 M. P. A., Roberts, D. G., Snelson, S. (eds) Salt tectonics: a global perspective. AAPG  
651 Memoir 65, 305-321.
- 652 Demercian, S., Szatmari, P., Cobbold, P. R. (1993). Style and pattern of salt diapirs  
653 due to thin-skinned gravitational gliding, Campos and Santos basins, offshore Brazil.  
654 *Tectonophysics*, 228(3-4), 393-433.
- 655 Davison, I., Anderson, L., Nuttall, P. (2012). Salt deposition, loading and gravity  
656 drainage in the Campos and Santos salt basins. *Geological Society of London Special  
657 Publications*, 363(1), 159-174.
- 658 Dooley, T. P., Hudec, M. R., Carruthers, D., Jackson, M. P., Luo, G. (2016). The effects  
659 of base-salt relief on salt flow and suprasalt deformation patterns—Part 1: Flow across  
660 simple steps in the base of salt. *Interpretation*, 5(1), SD1-SD23.
- 661 Dooley, T. P., Hudec, M. R. (2016). The effects of base-salt relief on salt flow and  
662 suprasalt deformation patterns—Part 2: Application to the eastern Gulf of Mexico.  
663 *Interpretation*, 5(1), SD25-SD38.
- 664 Dooley, T. P., Hudec, M. R., Pichel, L. M., Jackson, M. P. (2018). The impact of base-  
665 salt relief on salt flow and suprasalt deformation patterns at the autochthonous,  
666 paraautochthonous and allochthonous level: insights from physical models.  
667 *Geological Society, London, Special Publications*, 476, SP476-13.

668 Fiduk, J. C., Rowan, M. G. (2012). Analysis of folding and deformation within layered  
669 evaporites in Blocks BM-S-8 &-9, Santos Basin, Brazil. Geological Society, London,  
670 Special Publications, 363(1), 471-487.

671 Garcia, S. F., Letouzey, J., Rudkiewicz, J. L., Danderfer Filho, A., & de Lamotte, D. F.  
672 (2012). Structural modeling based on sequential restoration of gravitational salt  
673 deformation in the Santos Basin (Brazil). *Marine and Petroleum Geology*, 35(1), 337-  
674 353.

675 Ge, H., Jackson, M. P., Vendeville, B. C. (1997). Kinematics and dynamics of salt  
676 tectonics driven by progradation. *AAPG bulletin*, 81(3), 398-423.

677 Gemmer, L., Ings, S.J., Medvedev, S. Beaumont, C. (2004). Salt tectonics driven by  
678 differential sediment loading: stability analysis and finite-element experiments. *Basin*  
679 *Research*, 16(2), 199-218.

680 Giles, K. A., & Rowan, M. G. (2012). Concepts in halokinetic-sequence deformation  
681 and stratigraphy. Geological Society, London, Special Publications, 363(1), 7-31.

682 Guerra, M. C., Underhill, J. R. (2012). Role of halokinesis in controlling structural styles  
683 and sediment dispersal in the Santos Basin, offshore Brazil. Geological Society,  
684 London, Special Publications, 363(1), 175-206.

685 Hadler-Jacobsen, F., Groth, A., Hearn, R.E., and Liestøl, F.M. (2010), Controls on and  
686 expressions of submarine fan genesis within a high accommodation margin setting,  
687 Santos Basin, Brazil—A high-resolution seismic stratigraphic and geomorphic case  
688 study, in Wood, L.J., Simo, T.T., and Rosen, N.C., eds., *Seismic Imaging of*  
689 *Depositional and Geomorphic Systems: Gulf Coast Section Society for Sedimentary*  
690 *Geology Foundation Annual Bob F. Perkins Research Conference Proceedings*, v. 30,  
691 p. 572–615.

692 Hossack, J. (1995). Geometric rules of section balancing for salt structures.

693 Hudec, M. R., Jackson, M. P. A. (2004). Regional restoration across the Kwanza  
694 Basin, Angola: Salt tectonics triggered by repeated uplift of a metastable passive  
695 margin. *AAPG bulletin*, 88(7), 971-990.

696 Hudec, M. R., & Norton, I. O. (2019). Upper Jurassic structure and evolution of the  
697 Yucatán and Campeche subbasins, southern Gulf of Mexico. *AAPG Bulletin*, 103(5),  
698 1133-1151.

699 Hudec, M. R., Dooley, T. P., Peel, F. J., & Soto, J. I. (2019). Controls on the evolution  
700 of passive-margin salt basins: Structure and evolution of the Salina del Bravo region,  
701 northeastern Mexico. *Geological Society of America Bulletin*.

702 Jackson, M.P., Hudec, M.R. (2017). *Salt Tectonics: Principles and Practice*.  
703 Cambridge University Press.

704 Jackson, C. A. L., Jackson, M. P., Hudec, M. R. (2015a). Understanding the  
705 kinematics of salt-bearing passive margins: A critical test of competing hypotheses for  
706 the origin of the Albian Gap, Santos Basin, offshore Brazil. *Geological Society of*  
707 *America Bulletin*, 127(11-12), 1730-1751.

708 Jackson, C. A. L., Jackson, M. P., Hudec, M. R., Rodriguez, C. R. (2015b). Enigmatic  
709 structures within salt walls of the Santos Basin—Part 1: Geometry and kinematics from  
710 3D seismic reflection and well data. *Journal of Structural Geology*, 75, 135-162.

711 Karner, G. D., Gambôa, L. A. P. (2007). Timing and origin of the South Atlantic pre-  
712 salt sag basins and their capping evaporites. *Geological Society, London, Special*  
713 *Publications*, 285(1), 15-35.

714 Krézsek, C., Adam, J. and Grujic, D (2007). Mechanics of fault and expulsion rollover  
715 systems developed on passive margins detached on salt: insights from analogue  
716 modelling and optical strain monitoring. *Geological Society, London, Special*  
717 *Publications*, 292(1), pp.103-121.

718 Lebit, H., Arasanipalai S., Tilton, J. & Ollagnon, P. (2019) Santos Vision: Innovative  
719 Seismic Data Processing in a Super Giant Oil Basin. *GeoExPro*, May, 2019.

720 Marton, G., Tari, G. Lehmann, C (1998). Evolution of salt-related structures and their  
721 impact on the post-salt petroleum systems of the Lower Congo Basin, offshore Angola.  
722 In: *American Association of Petroleum Geologists International Conference and*  
723 *Exhibition, Rio de Janeiro. Extended Abstracts Volume*, 834–834.



724 Meisling, K. E., Cobbold, P. R., Mount, V. S. (2001). Segmentation of an obliquely  
725 rifted margin, Campos and Santos basins, southeastern Brazil. AAPG bulletin, 85(11),  
726 1903-1924.

727 Modica, C. J., Brush, E. R., 2004. Postrift sequence stratigraphy, paleogeography, and  
728 fill history of the deep-water Santos Basin, offshore southeast Brazil. AAPG bulletin,  
729 88(7), 923-945.

730 Mohriak, W.U., Macedo, J.M., Castellani, R.T., Rangel, H.D., Barros, A.Z.N., Latgé,  
731 M.A.L., Mizusaki, A.M.P., Szatmari, P., Demercian, L.S., Rizzo, J.G. Aires, J.R.  
732 (1995). Salt tectonics and structural styles in the deep-water province of the Cabo Frio  
733 region, Rio de Janeiro, Brazil, *in*: Jackson, M. P. A., Roberts, D. G., Snelson, S. (eds)  
734 Salt tectonics: a global perspective. AAPG Memoir 65, 273-304.

735 Mohriak, W., Nemčok, M., Enciso, G. (2008). South Atlantic divergent margin  
736 evolution: rift-border uplift and salt tectonics in the basins of SE Brazil. Geological  
737 Society, London, Special Publications, 294(1), 365-398.

738 Mohriak, W. U., Nóbrega, M., Odegard, M. E., Gomes, B. S., & Dickson, W. G. (2010).  
739 Geological and geophysical interpretation of the Rio Grande Rise, south-eastern  
740 Brazilian margin: extensional tectonics and rifting of continental and oceanic crusts.

741 Mohriak, W. U., Szatmari, P., Anjos, S. (2012). Salt: geology and tectonics of selected  
742 Brazilian basins in their global context. Geological Society, London, Special  
743 Publications, 363(1), 131-158.

744 Patruno, S., Hampson, G. J., & Jackson, C. A. (2015). Quantitative characterisation of  
745 deltaic and subaqueous clinoforms. Earth-Science Reviews, 142, 79-119.

746 Peel, F. J. (2014). The engines of gravity-driven movement on passive margins:  
747 Quantifying the relative contribution of spreading vs. gravity sliding mechanisms.  
748 Tectonophysics, 633, 126-142.

749 Pichel, L. M., Peel, F., Jackson, C.A.-L., Huuse, M., 2018, Geometry and kinematics  
750 of salt-detached ramp syncline basins, Journal of Structural Geology, 115, 208-230.  
751 in press, doi: 10.1016/j.jsg.2018.07.016.

752 Pichel, L. M., Huuse, M., Redfern, J., & Finch, E. (2019a). The influence of base-salt  
753 relief, rift topography and regional events on salt tectonics offshore Morocco. *Marine*  
754 *and Petroleum Geology*, 103, 87-113.

755 Pichel, L. M., Finch, E., & Gawthorpe, R. L. (2019b). The Impact of Pre-Salt Rift  
756 Topography on Salt Tectonics: A Discrete-Element Modeling Approach. *Tectonics*,  
757 38(4), 1466-1488.

758 Pichel, L. M., Jackson, C. A. L., Peel, F., & Dooley, T. P. (2019c). Base-salt relief  
759 controls salt-tectonic structural style, São Paulo Plateau, Santos Basin, Brazil. *Basin*  
760 *Research*.

761 Pichel, L. M., & Jackson, C. A-L., (2020) Four-dimensional Variability of Composite  
762 Halokinetic Sequences. *Basin Research*.

763 Quirk, D. G., Schødt, N., Lassen, B., Ings, S. J., Hsu, D., Hirsch, K. K., Von Nicolai, C.  
764 (2012). Salt tectonics on passive margins: examples from Santos, Campos and  
765 Kwanza basins. *Geological Society, London, Special Publications*, 363(1), 207-244.

766 Quirk, D. G., & Pilcher, R. S. (2012). Flip-flop salt tectonics. *Geological Society*,  
767 *London, Special Publications*, 363(1), 245-264.

768 Roberts, A. M., Kusznir, N. J., Yielding, G., & Styles, P. (1998). 2D flexural  
769 backstripping of extensional basins; the need for a sideways glance. *Petroleum*  
770 *Geoscience*, 4(4), 327-338.

771 Rodriguez, C. R., Jackson, C. L., Rotevatn, A., Bell, R. E., Francis, M. (2019). Dual  
772 tectonic-climatic controls on salt giant deposition in the Santos Basin, offshore Brazil.  
773 *Geosphere*, 14(1), 215-242.

774 Rowan, M. G., Lawton, T. F., Giles, K. A., & Ratliff, R. A. (2003). Near-salt deformation  
775 in La Popa basin, Mexico, and the northern Gulf of Mexico: A general model for  
776 passive diapirism. *AAPG bulletin*, 87(5), 733-756.

777 Rowan, M. G., Peel, F. J., & Vendeville, B. C. (2004). Gravity-driven fold-belts on  
778 passive margins.

779 Rowan, M. G., & Ratliff, R. A. (2012). Cross-section restoration of salt-related  
780 deformation: Best practices and potential pitfalls. *Journal of Structural Geology*, 41,  
781 24-37.

782 Rowan, M. G., Giles, K. A., Hearon IV, T. E., Fiduk, J. C. (2016). Megaflaps adjacent  
783 to salt diapirs. *AAPG Bulletin*, 100(11), 1723-1747.

784 Sclater, J. G., & Christie, P. A. (1980). Continental stretching: An explanation of the  
785 post-mid-Cretaceous subsidence of the central North Sea basin. *Journal of*  
786 *Geophysical Research: Solid Earth*, 85(B7), 3711-3739.

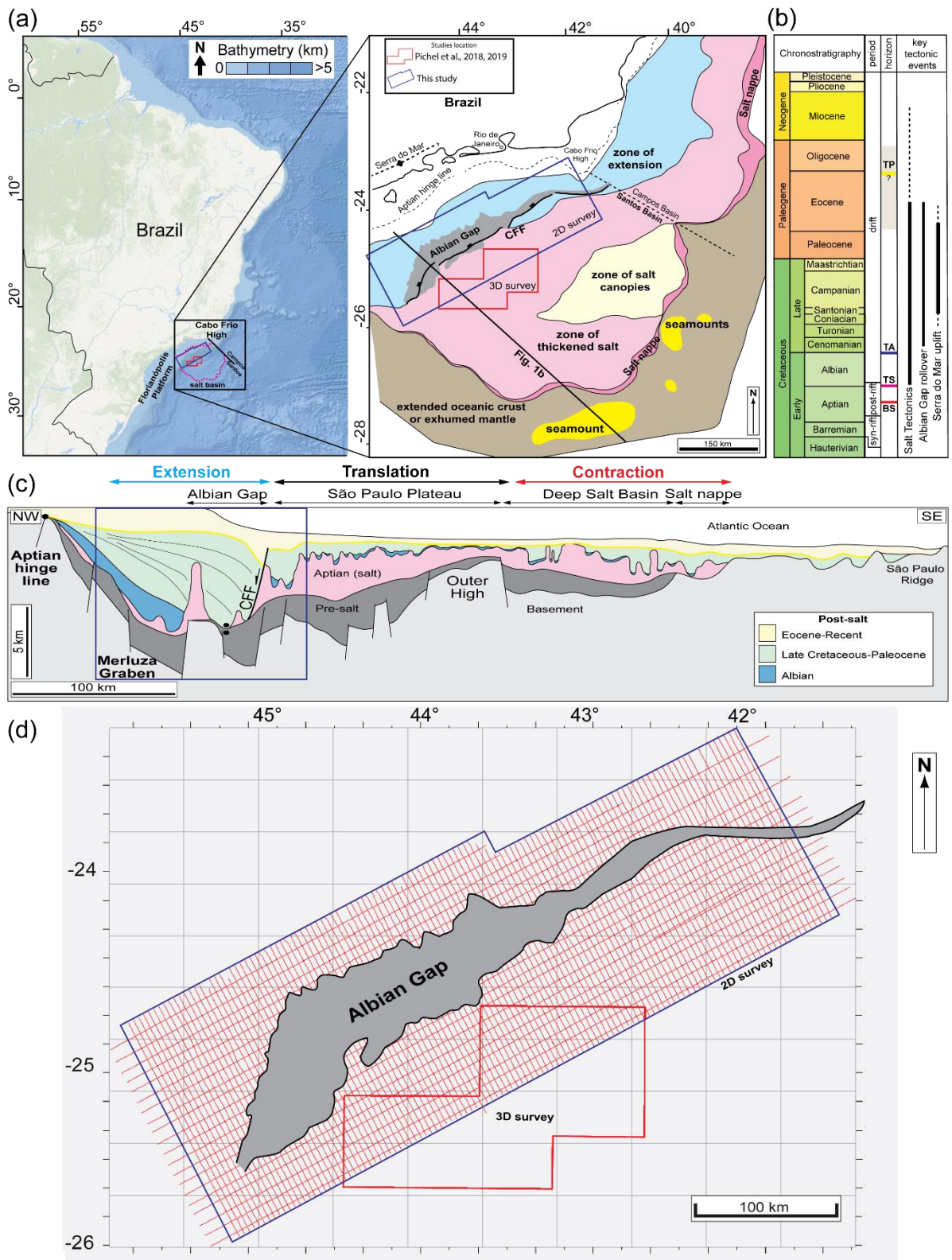
787 Scotchman, I. C., Marais-Gilchrist, G., Souza, F., Chaves, F. F., Atterton, L. A.,  
788 Roberts, A., & Kuszniir, N. J. (2006). A failed sea-floor spreading centre, Santos Basin,  
789 Brasil. In *Rio Oil & Gas Expo and Conference*. Rio de Janeiro, Brazil, Brazilian  
790 Petroleum, Gas and Biofuels Institute.

791 Scotchman, I. C., Gilchrist, G., Kuszniir, N. J., Roberts, A. M., & Fletcher, R. (2010).  
792 The breakup of the South Atlantic Ocean: formation of failed spreading axes and  
793 blocks of thinned continental crust in the Santos Basin, Brazil and its consequences  
794 for petroleum system development. In *Geological Society, London, Petroleum*  
795 *Geology Conference series* (Vol. 7, No. 1, pp. 855-866). Geological Society of London.

796 Szatmari, P. M. C. M., Guerra, M. C. M., & Pequeno, M. A. (1996). Genesis of large  
797 counter-regional normal fault by flow of Cretaceous salt in the South Atlantic Santos  
798 Basin, Brazil. *Geological Society, London, Special Publications*, 100(1), 259-264.

799 Vendeville, B. C., Jackson, M. P. A. (1992). The rise of diapirs during thin-skinned  
800 extension. *Marine and Petroleum Geology*, 9(4), 331-354.

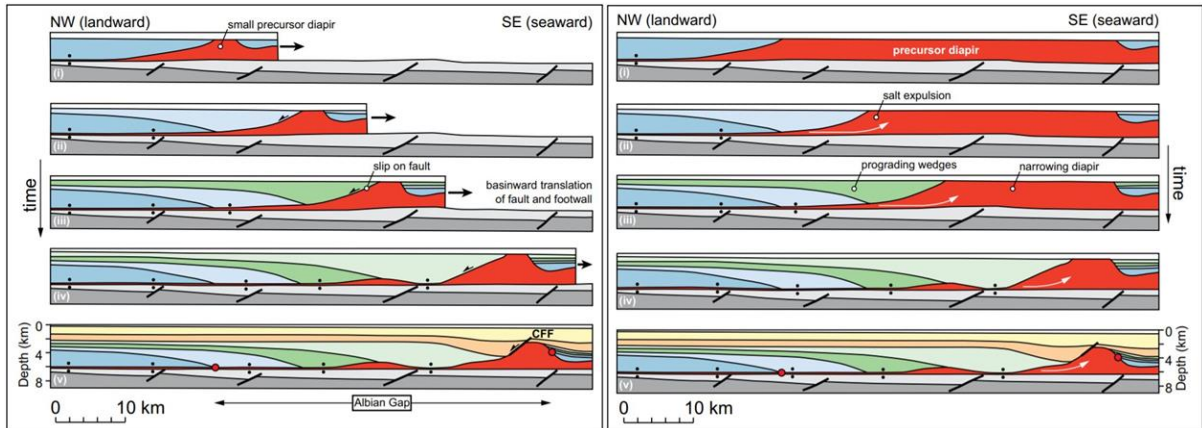
801 **FIGURES**



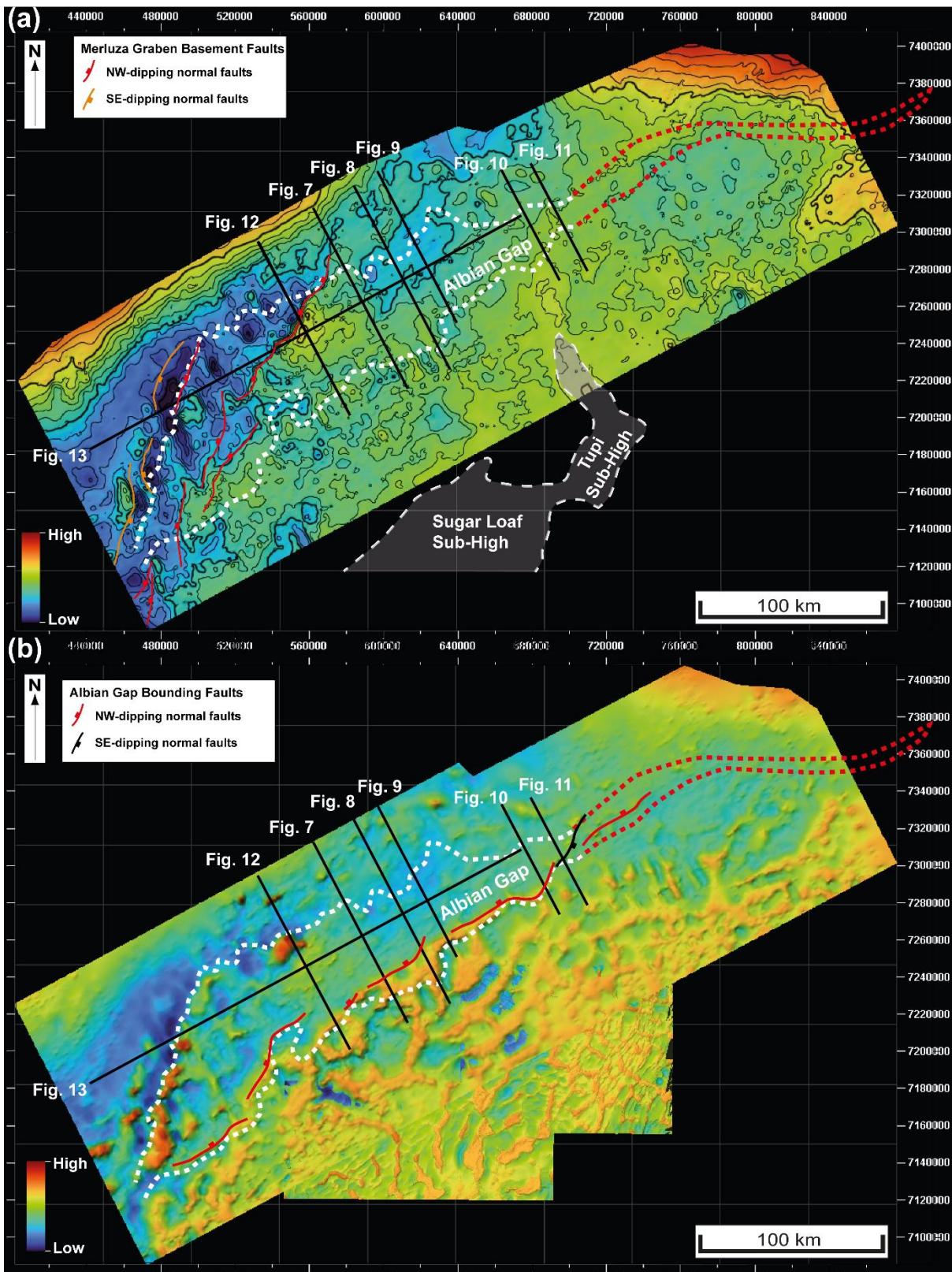
802

803 Fig. 1: (a) Bathymetry and structural maps showing the regional salt-related structural domains  
 804 offshore SE Brazil including a new outline of the Albian Gap. (b) Chrono-stratigraphic chart  
 805 illustrating the main horizons mapped in this study and timing of relevant tectonic events in  
 806 the basin (adapted from Davison et al., 2012). (c) Regional geoseismic cross-section showing

807 the main regional salt-related structural domains offshore the Santos Basin (adapted from  
 808 Jackson et al., 2015b). Location of the study-area and seismic survey used in the study are  
 809 shown by a blue polygon in (a) and (c). (d) 2D and 3D seismic survey used in the study and  
 810 outline of the Albian Gap. In (a) and (b), CFF corresponds to the Albian Gap bounding fault,  
 811 the Cabo Frio Fault.



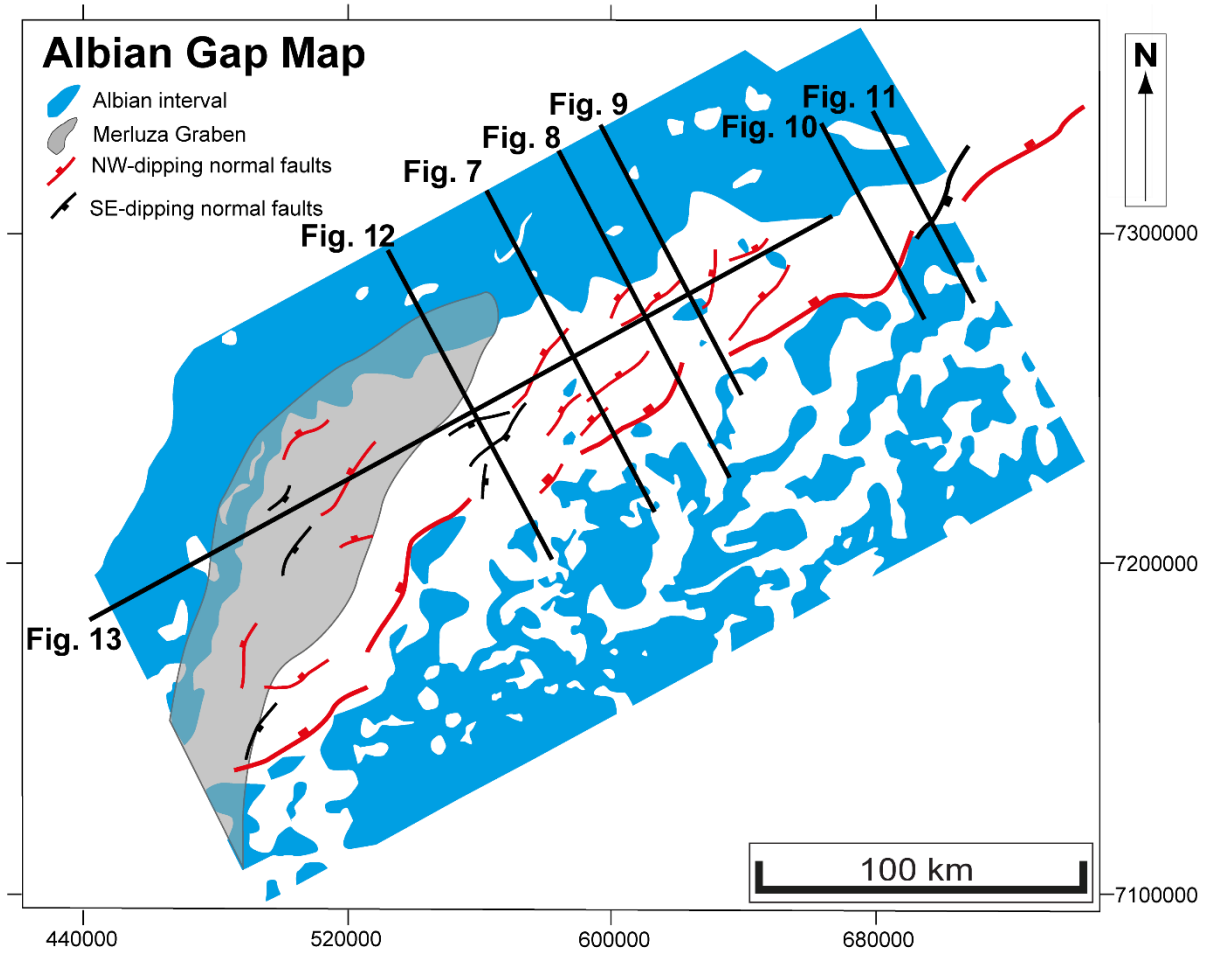
812  
 813 *Fig. 2: Competing end-member models of the origin and evolution of the Albian Gap: (a) post-*  
 814 *Albian extension; (b) post-Albian salt expulsion and basinward inflation (adapted from Rowan*  
 815 *and Ratliff, 2012, no vertical exaggeration). Note flat datum during each restoration step. Red*  
 816 *dots indicate the limits of the Albian interval and, thus, the extent of the Albian Gap.*



817

818 Fig. 3: (a) Base-salt map showing the location of main pre-salt rift faults associated with the  
 819 Merluza Graben and the Tupi and Sugar-Loaf Sub-Highs (cf. Pichel et al., 2019) downdip from  
 820 the study-area. (b) Top-Salt map showing the distribution of main salt-detached thin-skinned

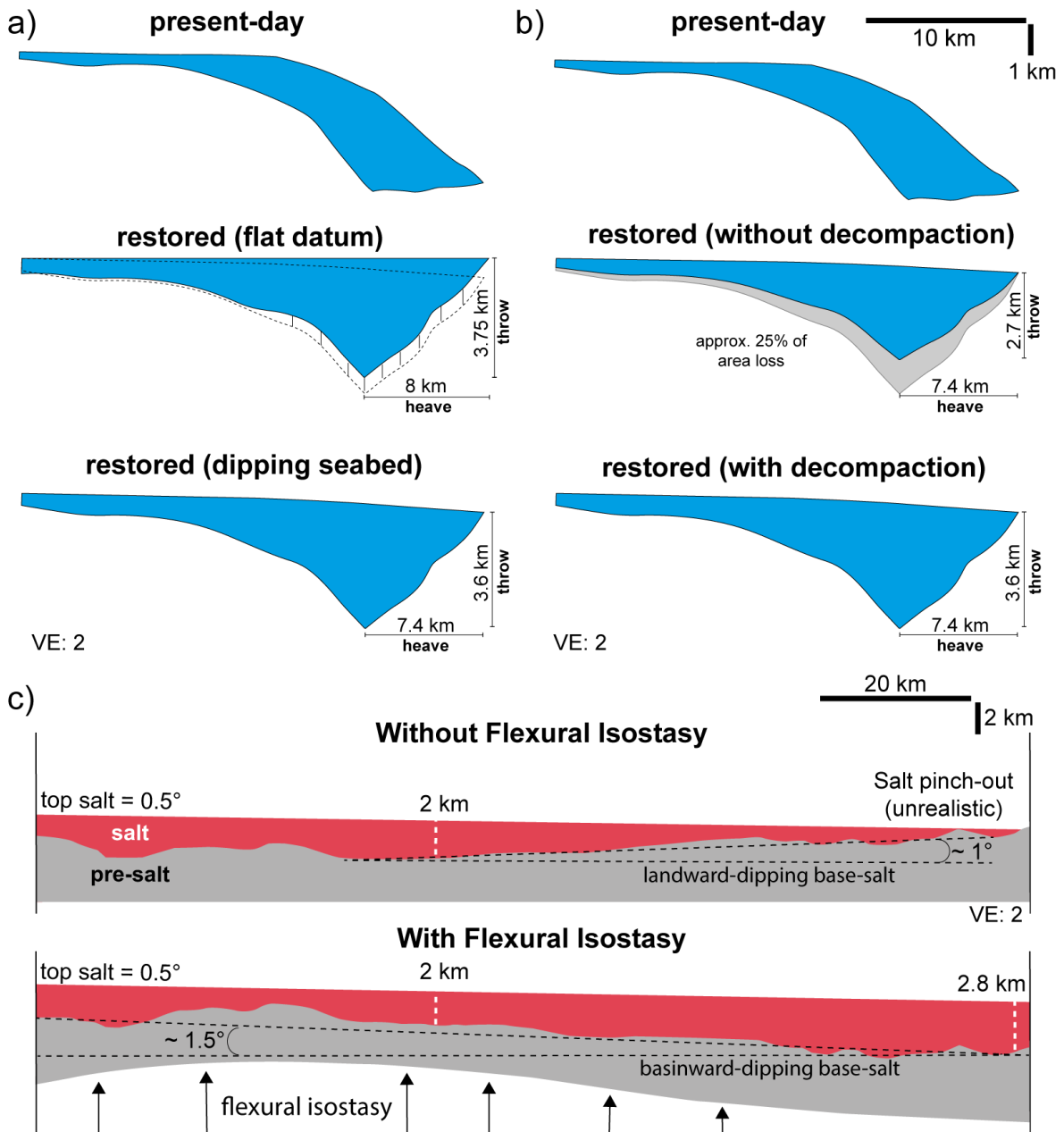
821 normal faults within the Albian Gap. Outline of the Albian Gap in dashed lines and seismic  
822 sections presented in the study in black.



823  
824 *Figure 4: Map showing the distribution of the Albian interval and outline of the Albian Gap. The*  
825 *pre-salt Merluza Graben and the main thin-skinned salt-detached normal faults associated*  
826 *with the Albian Gap rollover are also indicated. Note remnants of the Albian interval within the*  
827 *gap in its central-north portion.*

828  
829  
830

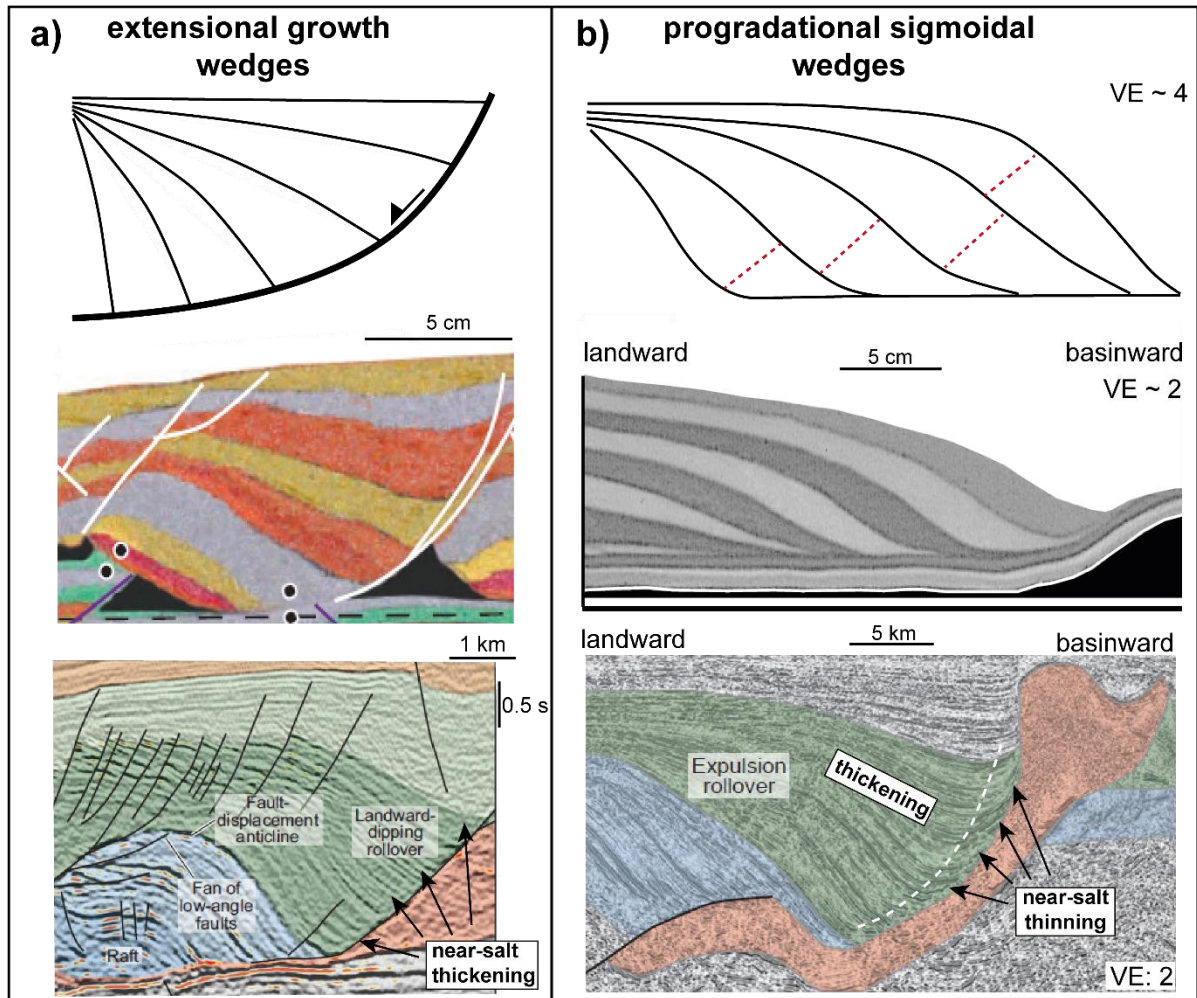




831

832 *Figure 5: Synthetic diagram comparing restoration workflows and illustrating the novel and*  
 833 *more geologically realistic approaches utilized in the study. (a) Comparison between rollover*  
 834 *wedges being restored to a flat-datum (previous studies, see fig. 2) and to a gently-dipping*  
 835 *seabed (this study). The former overestimates extension as the throw and heave are larger*  
 836 *than when restoring these sequences to a gently-dipping slope bathymetry. (b) Same wedge*  
 837 *from (a) is restored with and without decompaction for comparison. There is c. 25% of loss in*  
 838 *area/volume, and thus overall thickness as well as less throw (c 1.1 km) when decompaction*  
 839 *is not incorporated in the workflow. (c) Comparison between restorations without (previous*  
 840 *studies) and with flexural isostasy (this study), in which the isostatic effects caused by*  
 841 *differential loading are observed. In the former, the base-salt remains the same and presents*

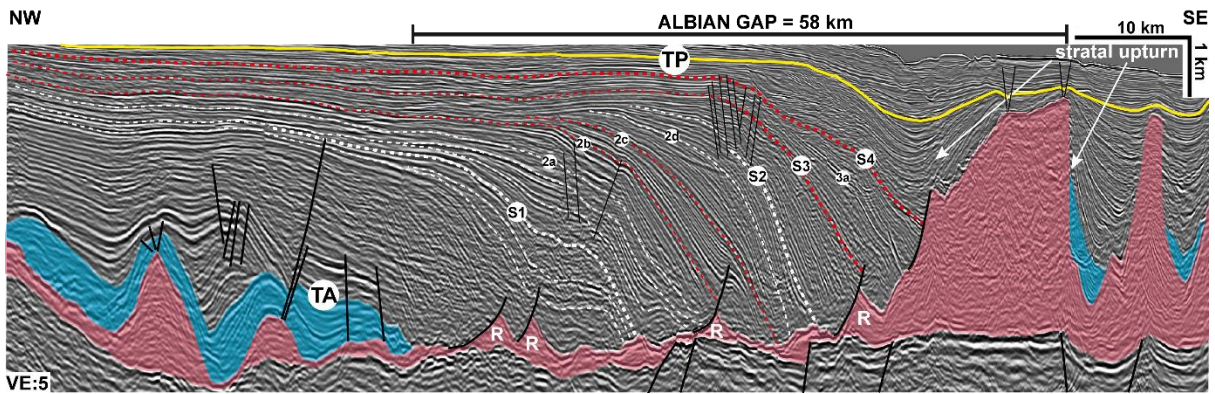
842 an anomalous landward dip throughout the entire workflow, which results also in unrealistic  
 843 distal salt thicknesses. In the latter, the base-salt gradually changes through time and switches  
 844 back to a more realistic initial basinward dip resulting also in more reasonable salt thickness  
 845 through the section.



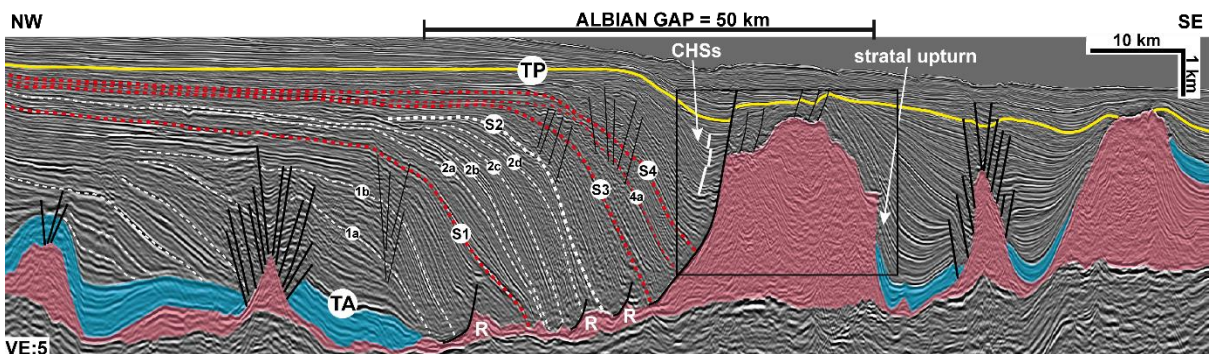
846  
 847 *Figure 6: Different styles of rollover growth wedges: a) basinward-thickening extensional*  
 848 *wedges with a physical model example in the second row (adapted from Jackson and Hudec,*  
 849 *2017) and a seismic example from the Kwanza Basin, Angola in the third-row (after Chimney*  
 850 *and Kluth, 2002 and Jackson and Hudec, 2017), and b) basinward-thinning cliniform*  
 851 *sigmoidal growth wedges with a physical model example in the second row (adapted from Ge*  
 852 *et al., 1997) and a seismic example from the Gulf of Mexico (adapted from Jackson and*  
 853 *Hudec, 2017).*

854

855

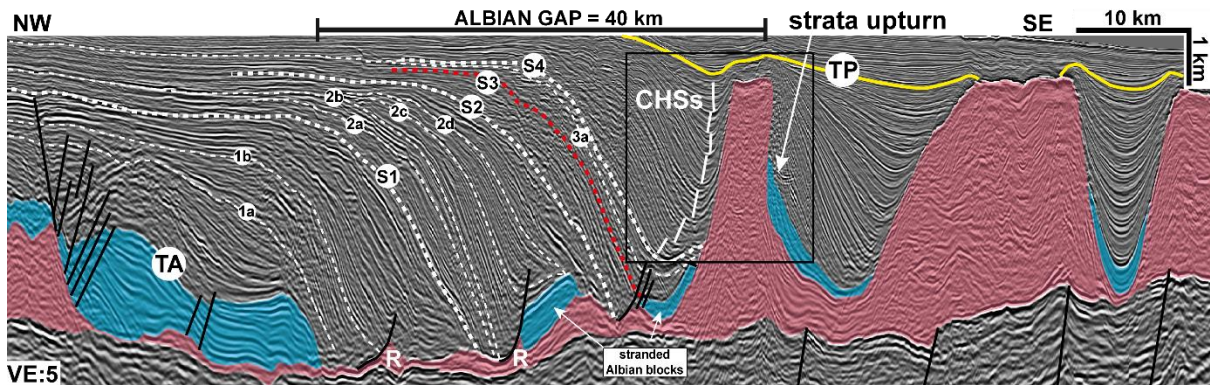


856  
 857 Figure 7: South-central dip-oriented section from the Albian Gap. Salt in pink, Albian in blue,  
 858 normal faults in black and an intra-Paleogene regional unconformity in yellow. The main post-  
 859 Albian rollover sequences are indicated by thick dashed lines and named S1-S4, intermediate  
 860 intervals are numbered and indicated by thin dashed lines for correlation purposes. The post-  
 861 Albian rollover presents contrasting growth wedges: expulsion-dominated basinward-thinning,  
 862 sigmoidal wedges (white) and extension-dominated basinward-thickening wedges (red). The  
 863 gap is 58 km wide being composed by a 50 km wide basinward-dipping rollover and an 8 km  
 864 wide salt wall with strata upturn on both its flanks. The gap is also associated with small  
 865 landward-dipping listric normal faults that become progressively younger basinward. Small  
 866 salt rollers indicated by (R). Seismic data courtesy of TGS and WesternGeco.



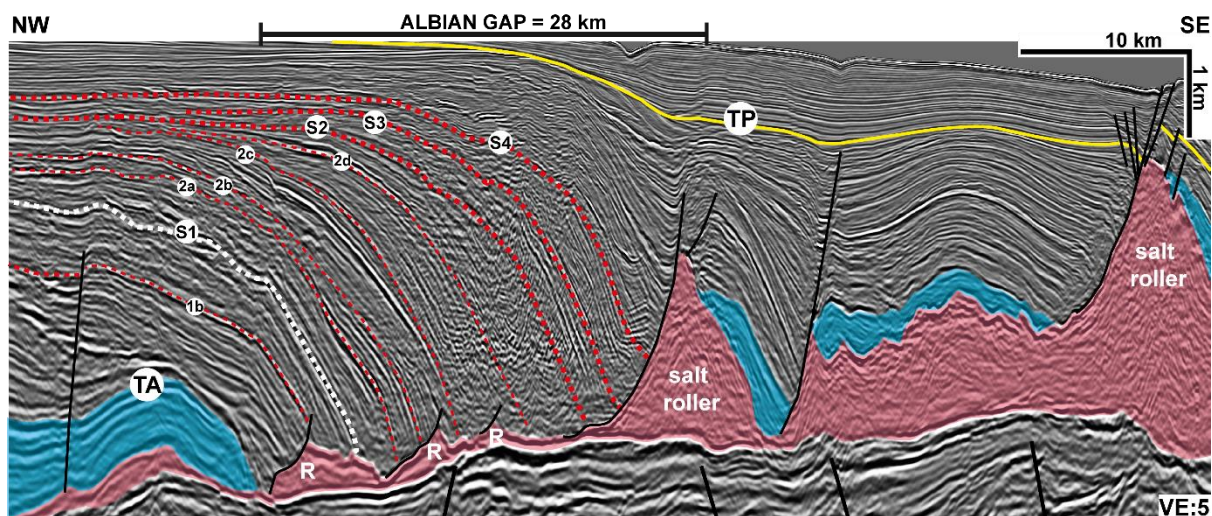
867  
 868 Figure 8: Central dip-oriented section from the Albian Gap. Salt in pink, Albian in blue, normal  
 869 faults in black and an intra-Paleogene regional unconformity in yellow. The main post-Albian  
 870 rollover sequences are indicated by thick dashed lines and named S1-S4, intermediate  
 871 intervals are numbered and indicated by thin dashed lines for correlation purposes. The post-  
 872 Albian rollover presents contrasting growth wedges: expulsion-dominated sigmoidal wedges  
 873 (white) and extension-dominated basinward-thickening wedges (red). The gap is 50 km wide  
 874 being composed of a 40 km wide basinward-dipping rollover and a 10 km wide salt wall with  
 875 strata upturn and halokinetic sequences (thick white lines) on its flanks and a large landward-  
 876 dipping normal fault on its landward side. The gap is also associated with small landward-  
 877 dipping listric normal faults that become progressively younger basinward. Small salt rollers

878 indicated by (R). Seismic data courtesy of TGS and WesternGeco. Black square represents  
 879 the zoomed-in section of figure 15.



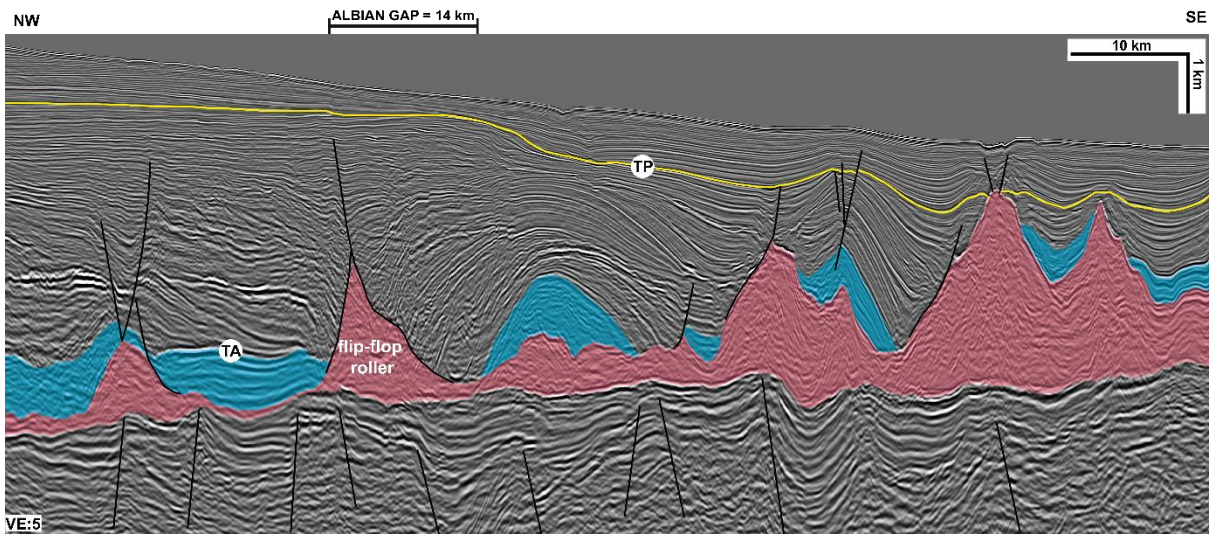
880  
 881 Figure 9: North-central dip-oriented section from the Albian Gap. Salt in pink, Albian in blue,  
 882 normal faults in black and an intra-Paleogene regional unconformity in yellow. The main post-  
 883 Albian rollover sequences are indicated by thick dashed lines and named S1-S4, intermediate  
 884 intervals are numbered and indicated by thin dashed lines for correlation purposes. The post-  
 885 Albian rollover presents contrasting growth wedges: expulsion-dominated sigmoidal wedges  
 886 (white) and extension-dominated basinward-thickening wedges (red). The gap is 40 km wide  
 887 being composed of a 37 km wide basinward-dipping rollover and 3 km wide salt wall with strata  
 888 upturn and halokinetic sequences (thick white lines) on its flanks. The gap is also associated  
 889 with small landward-dipping listric normal faults that become progressively younger basinward  
 890 and occasionally downlap remnant Albian blocks. Small salt rollers indicated by (R). Seismic  
 891 data courtesy of TGS and WesternGeco. Black square represents the zoomed-in section of  
 892 figure 15.

893

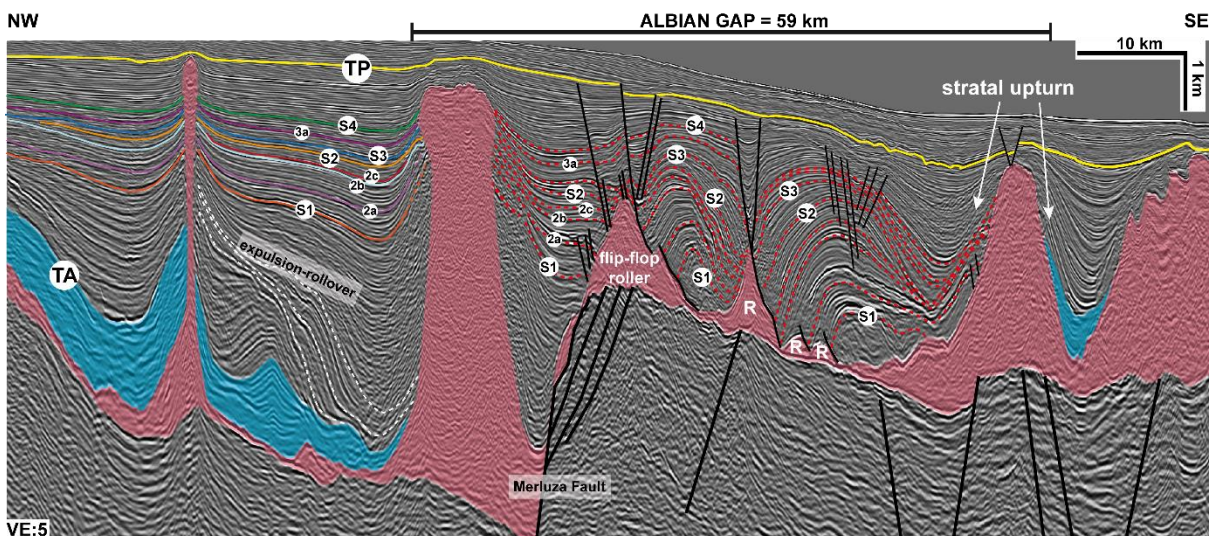


894  
 895 Figure 10: North dip-oriented section from the Albian Gap. Salt in pink, Albian in blue, normal  
 896 faults in black and an intra-Paleogene regional unconformity in yellow. The main post-Albian

897 rollover sequences are indicated by thick dashed lines and named S1-S4, intermediate  
 898 intervals are numbered and indicated by thin dashed lines for correlation purposes. The gap  
 899 is 28 km wide being composed of a 27 km wide basinward-dipping rollover and c.1 km wide  
 900 reactive (extensional) salt wall/roller defined by a large landward-dipping normal fault. The  
 901 post-Albian rollover is dominated by basinward-thickening, extensional wedges (red dashed  
 902 lines) associated with small landward-dipping listric normal faults that become progressively  
 903 younger basinward. Only one expulsion-dominated sigmoidal wedge is observed (white  
 904 dashed line) in the lower sequences. Small salt rollers indicated by (R). Seismic data courtesy  
 905 of TGS and WesternGeco.

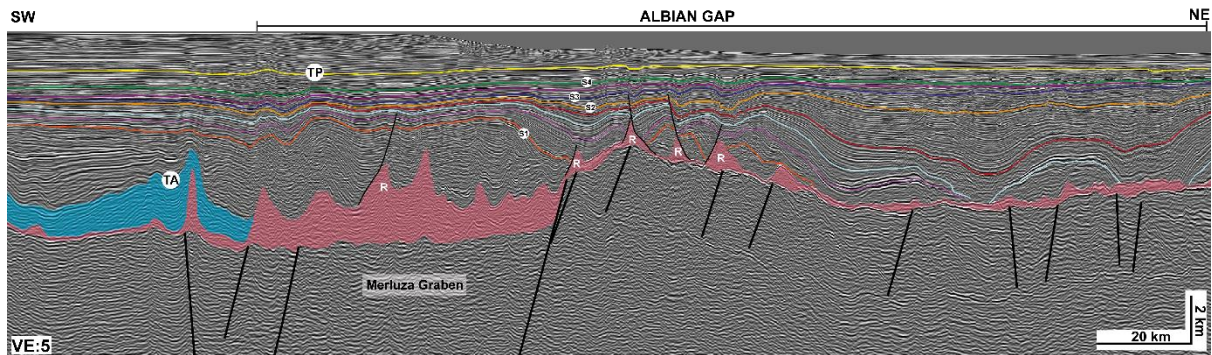


906  
 907 Figure 11: Northernmost section illustrating the switch in fault polarity associated with a flip-  
 908 flop salt reactive diapir bounding the Albian Gap. The gap is significantly narrower (14 km)  
 909 and associated with a wide 35 km wide extensional turtle anticline further downdip. Seismic  
 910 data courtesy of TGS and WesternGeco.

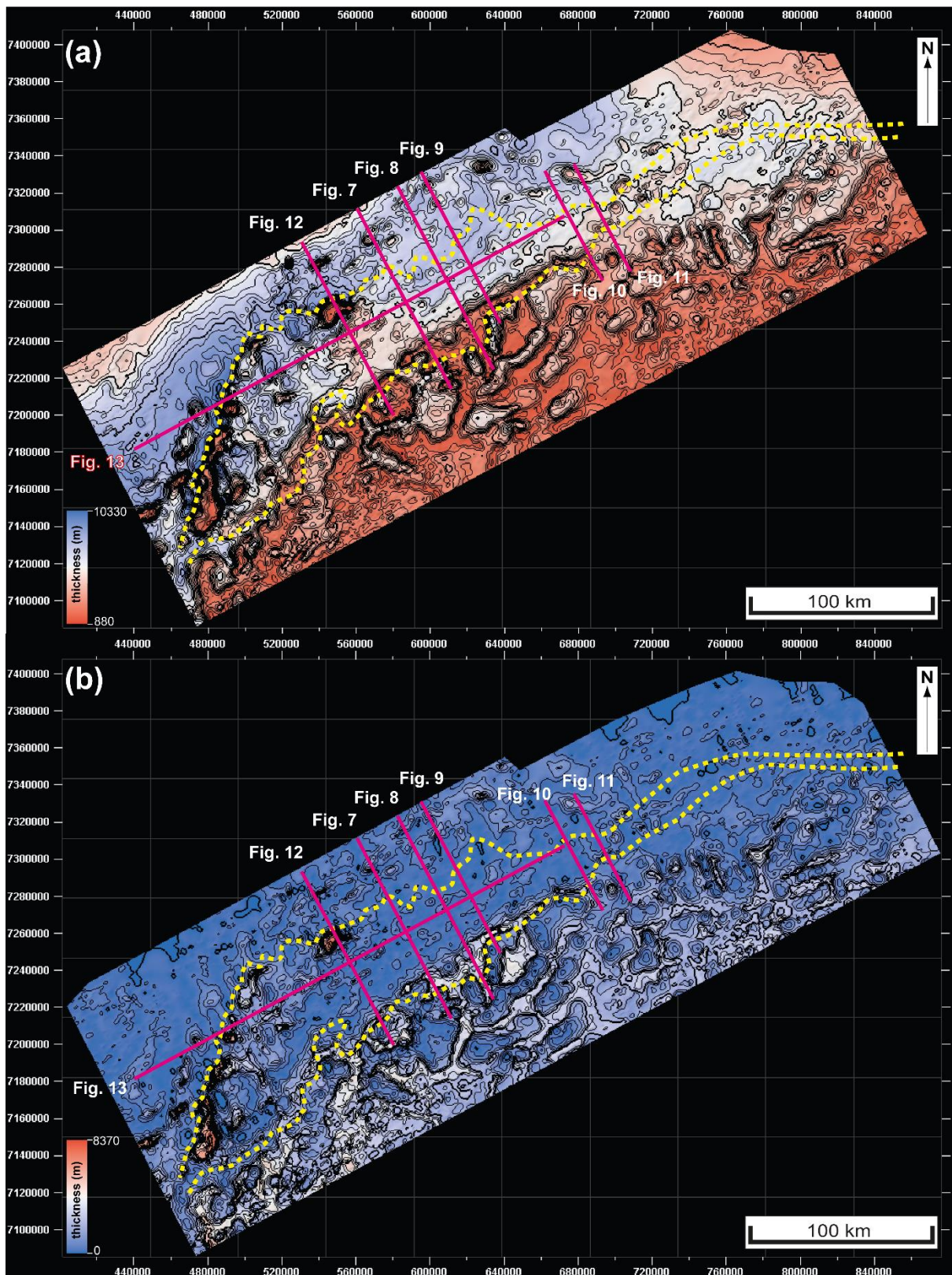


911  
 912 Figure 12: Central dip-oriented section from the Albian Gap. Salt in pink, Albian in blue and

913 normal faults in black. An intra-Paleogene regional unconformity in yellow. The main post-  
 914 Albian rollover sequences are indicated by thick dashed lines and named S1-S4, intermediate  
 915 intervals are numbered and indicated by thin dashed lines for correlation purposes. The gap  
 916 is 58 km wide. It comprises the downdip edge of the Merluza Graben and a 8 km, 8.5 km tall  
 917 salt stock at its hangingwall. Further downdip the Albian Gap is defined by two large salt rollers,  
 918 the updip one with a flip-flop geometry. Basinward-dipping listric normal faults and extensional  
 919 wedges dominate the post-Albian rollover sequence. In this case, extensional wedges are  
 920 dominantly landward-thickening (red dashed lines). Expulsion-driven sigmoidal wedges (white  
 921 dashed lines) occur only updip of the Albian Gap, within the Merluza Graben. Downdip, the  
 922 Albian Gap is bounded by a diapir that shows significant strata upturn on both flanks.. Small  
 923 salt rollers indicated by (R). Seismic data courtesy of TGS and WesternGeco.

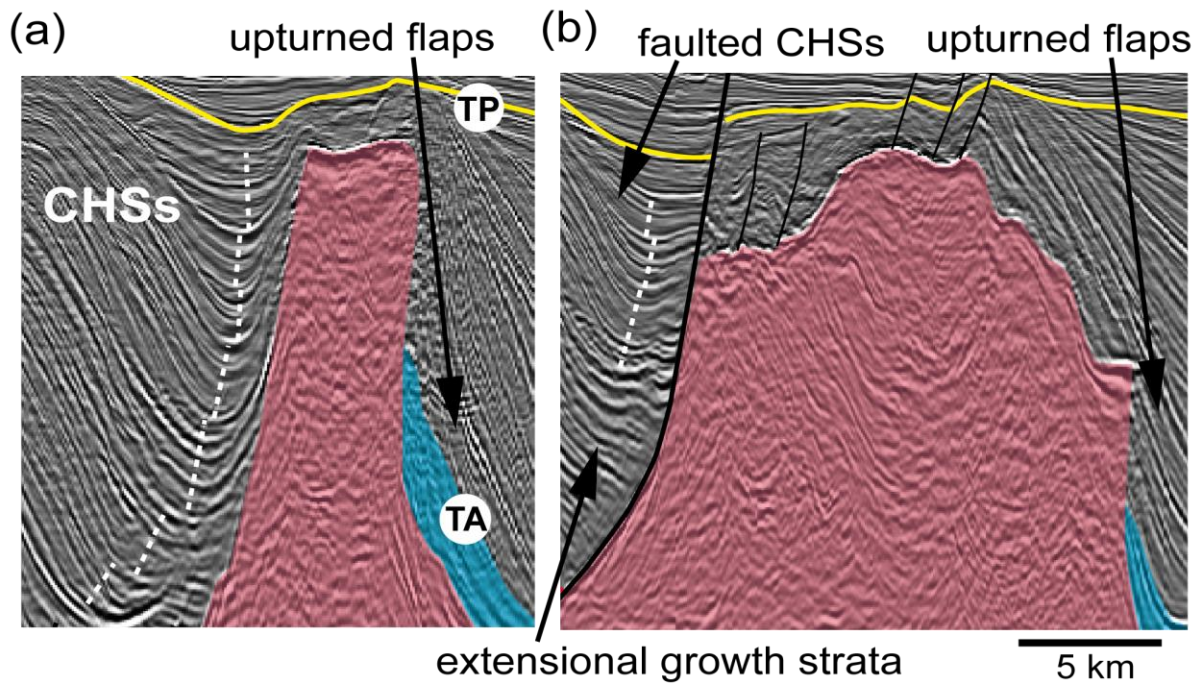


924  
 925 *Figure 13: Strike-section illustrating the thickness variations with the Albian Gap and its*  
 926 *relationship with the Merluza Graben to the south. Salt in pink, Albian in blue, normal faults in*  
 927 *black and an intra-Paleogene regional unconformity in yellow. Salt rollers are indicated by (R).*  
 928 *The overburden is 9-10 km to the south, with the post-Albian rollover being up to 9 km thick;*  
 929 *whereas to the north it is on average 6-7 km thick. The main post-Albian rollover sequences*  
 930 *are indicated by S1-S4 and with different colours as they vary alongs-strike between*  
 931 *expulsion- and extension-dominated in this section. Seismic data courtesy of TGS and*  
 932 *WesternGeco.*



933

934 *Figure 14: (a) Overburden thickness map and (b) salt thickness map. The maximum*  
 935 *overburden thickness (9-10 km) and thinner (>200m) salt occur in the proximal domain within*  
 936 *the Albian Gap. Albian Gap outline in yellow dashed line. Seismic profiles from figures 7-13*  
 937 *are numbered and shown by pink lines.*



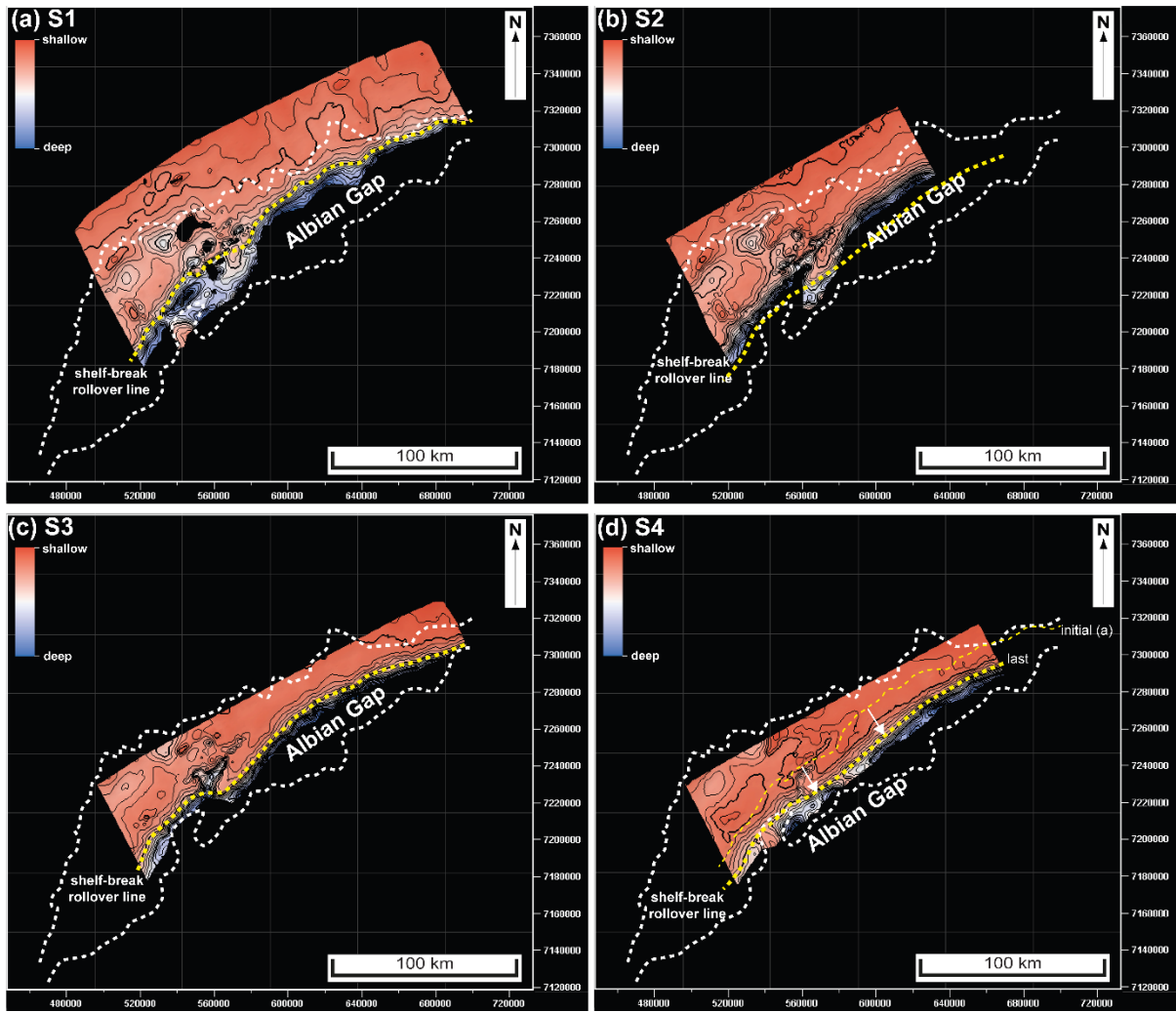
938

939 *Figure 15: Zoom of near-diapir upturned strata at the downdip edge of the Albian Gap. In (a),*  
 940 *zoom from figure 8 showing composite halokinetic sequences (CHSs) characterized by*  
 941 *localized (c. 1 km) of upturning and thinning on the landward flank of the diapir and larger*  
 942 *upturned flaps on its basinward flank. In (b), a significantly wider diapir presents similar*  
 943 *upturned flaps on its basinward flank. Its landward flank has a lower extensional rollover with*  
 944 *thickening towards the diapir and its bounding fault, whereas the upper section presents*  
 945 *characteristic upturn and stratal thinning of CHSs, being later offset due to propagation of the*  
 946 *lower normal fault.*

947

948

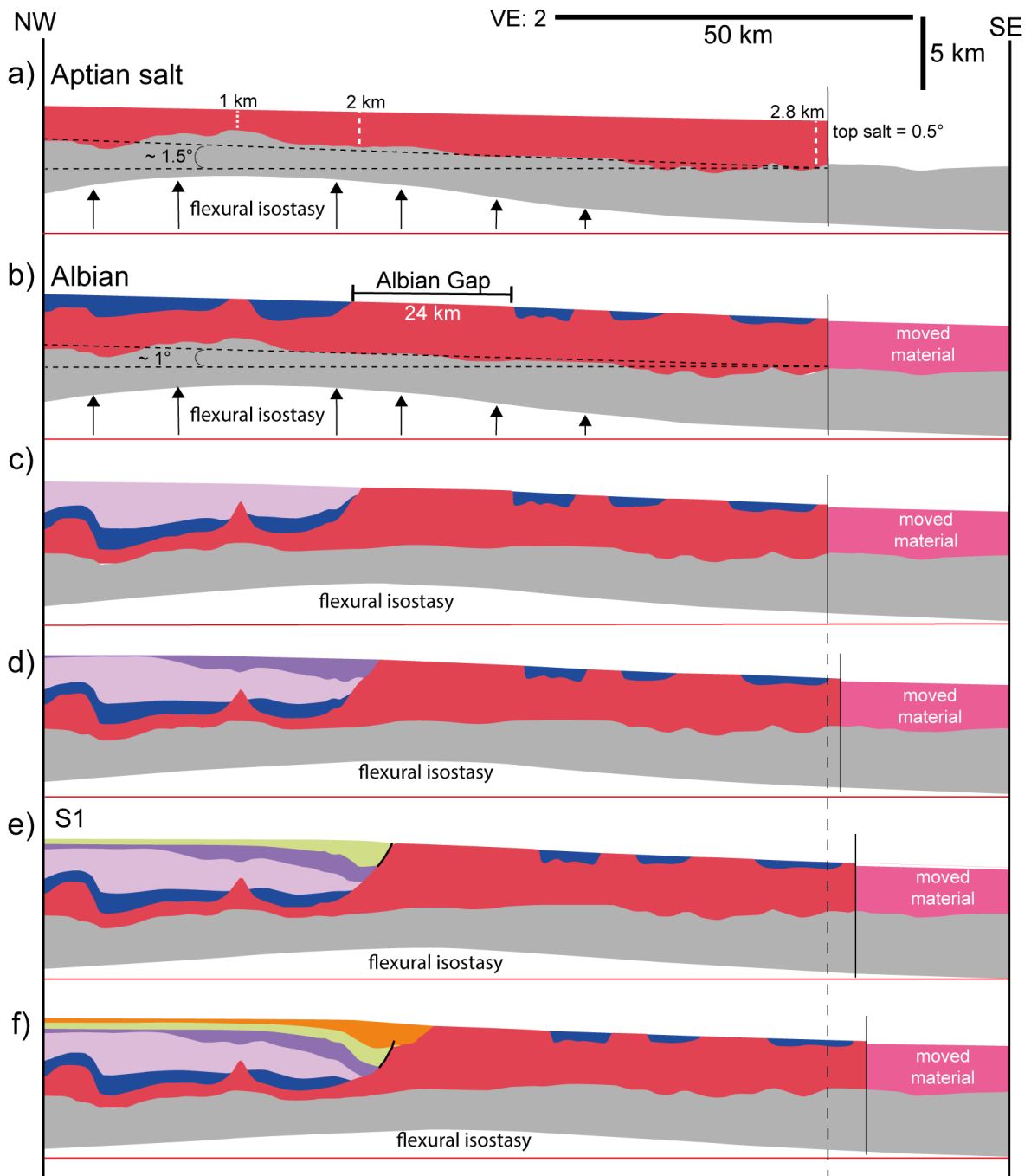


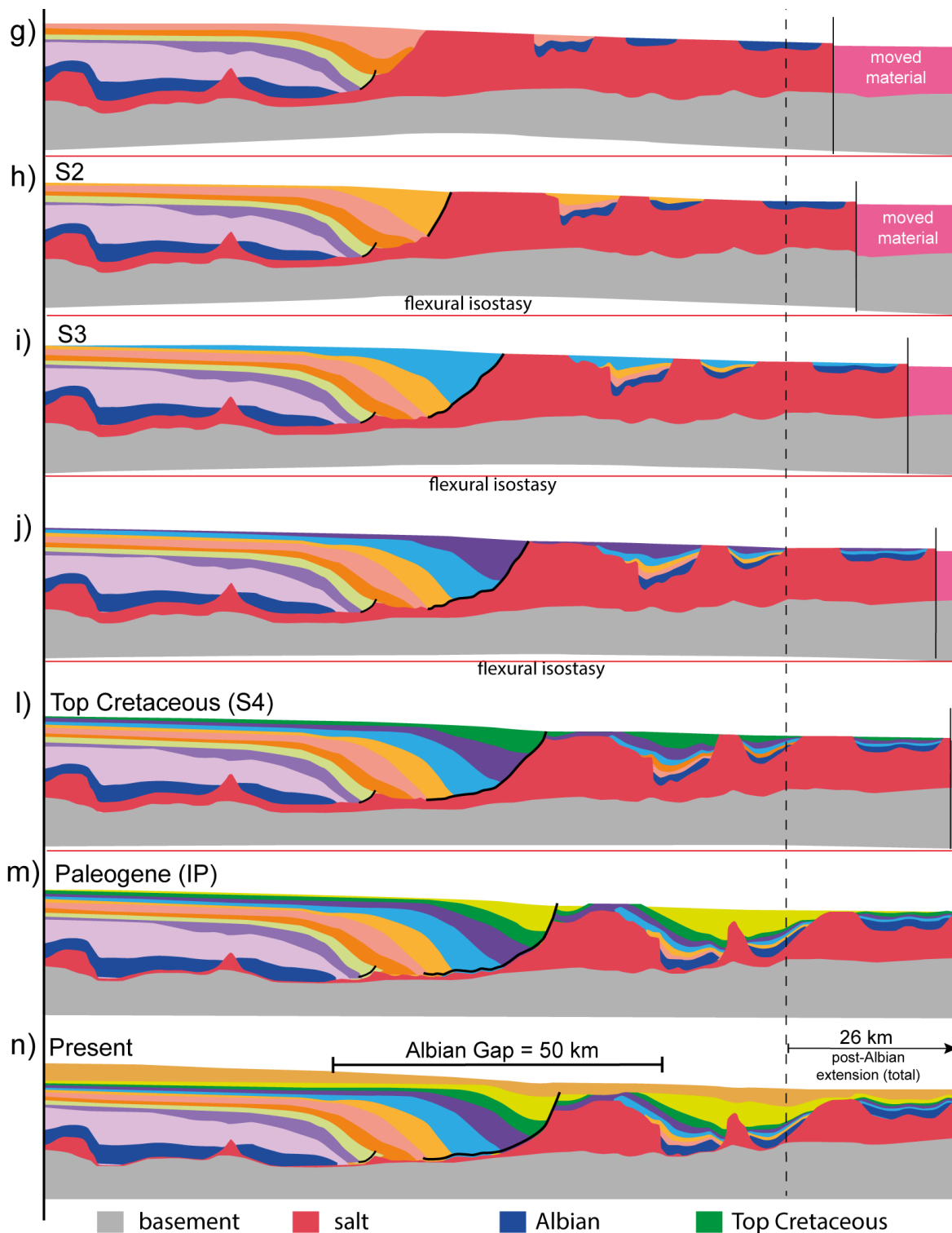


949

950 *Figure 16: Structural maps of key stratigraphic intervals within the post-Albian rollover in the*  
 951 *Albian Gap: (a) S1, (b) S2, (c) S3 and (d) S4 from cross-sections (figs. 7-13). The maps*  
 952 *demonstrate that in the central-south portion where the Albian gap is wider, the shelf-break*  
 953 *rollover point was located 14-20 km further basinward, indicating greater progradation of*  
 954 *sediments. White arrows indicate c. 20 km of shelf-break advance from the initial stages (top*  
 955 *S1) (a) to final stages (top-S4) (d) of margin progradation.*

956

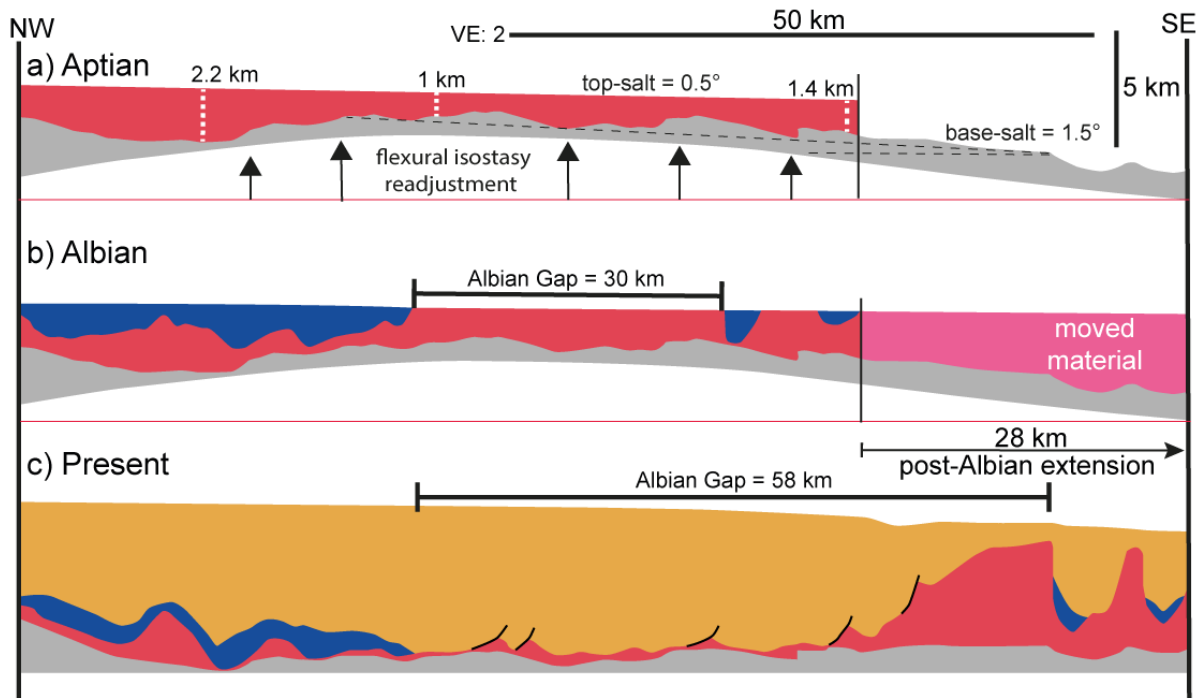




958

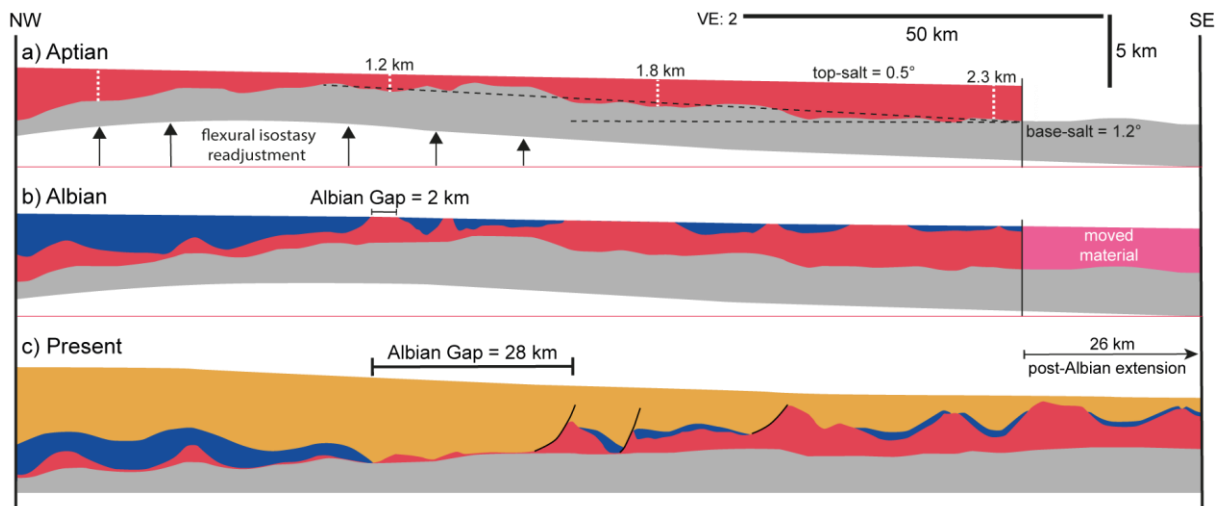
959 *Figure 17: Detailed sequential restoration of the central and most representative section from*  
 960 *the Albian Gap. The workflow involves decompaction, unfolding, move on fault and flexural*  
 961 *isostasy. Extension on each time-step is indicated by movement of the downdip end wall.*  
 962 *Decompaction and unfolding of post-Albian sequences (a-n) demonstrates that the Albian Gap*  
 963 *accommodated 26 km of post-Albian extension and that the gap was initially and partially*  
 964 *formed already during the Albian as a 24 km wide passive salt wall, resulting in a 50 km wide*

965 *Albian Gap at present. The restoration of the lowermost post-Albian sequences show little (c.*  
 966 *1 km, g-h, h-i, j-l) to no (l-m) extension, with deformation being dominated by differential*  
 967 *loading and salt expulsion. Conversely, the later sequences are dominated by extension and*  
 968 *movement over a large landward-dipping listric normal fault (b-f), although salt expulsion also*  
 969 *occur secondarily due to greater sediment loading on its hangingwall. During the Aptian (a)*  
 970 *and Albian (b), the base-salt dipped regionally >1° basinward but flipped gradually through*  
 971 *time during the deposition of the anomalously thick post-Albian rollover within the Albian Gap.*



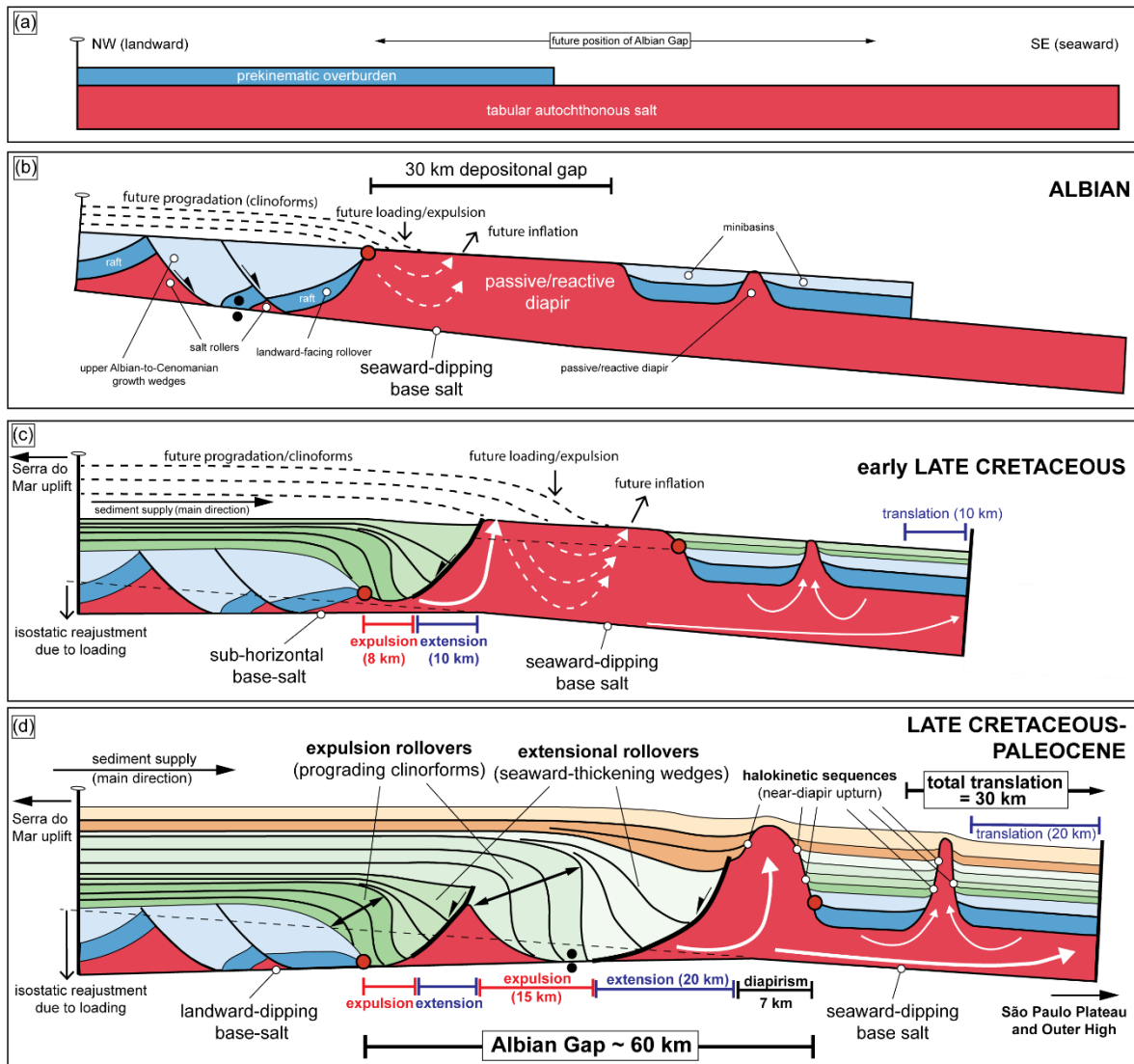
972

973 *Figure 18: Restoration of a section over the southern portion of the Albian Gap (Fig. 7) showing*  
 974 *dip reversal of the base-salt by flexural isostasy due to the deposition of a c. 6-7 km thick post-*  
 975 *Abian rollover (fig. 9). The Albian Gap is at present 58 km, resulting from a combination from*  
 976 *post-Albian extension (c. 28 km) and salt expulsion from a c. 30 km wide Albian salt wall.*



977

978 *Figure 19: Restoration of section over the northern portion of the Albian Gap showing dip*  
 979 *reversal of the base-salt by flexural isostasy due to the deposition of a c. 5 km thick post-Albian*  
 980 *rollover (fig. 10). The Albian Gap is at present 28 km, resulting primarily of post-Albian*  
 981 *extension (c. 26 km).*



982

983 *Figure 20: New kinematic model explaining the origin and evolution of the Albian Gap. (a-b)*  
 984 *During the Albian, salt deformation was controlled by salt detached extension with basinward-*  
 985 *dipping normal faults and development of a 30 km wide reactive/passive diapir downdip. (c)*  
 986 *During the early Late Cretaceous, margin-scale progradation of sediments over the earlier-*  
 987 *formed passive salt wall resulted in develop of small landward-dipping normal faults*  
 988 *(extension) and salt expulsion (differential loading) from the diapir onto the São Paulo Plateau*  
 989 *further downdip. (d) Continuous progradation resulted in further salt expulsion and extension*  
 990 *with development of larger landward-dipping faults and, consequently, salt inflation, diapirism*  
 991 *and translation further downdip. The normal faults became progressively younger basinward*  
 992 *and larger through time as a consequence of gradual landward-rotation of the base-salt driven*  
 993 *by base-salt isostatic readjustment in response to the greater loading within the Albian Gap.*